The 1990 Edward Campbell Memorial Lecture
ASM INTERNATIONAL

Behavior of Metal Alloys in the Semisolid State

MERTON C. FLEMINGS

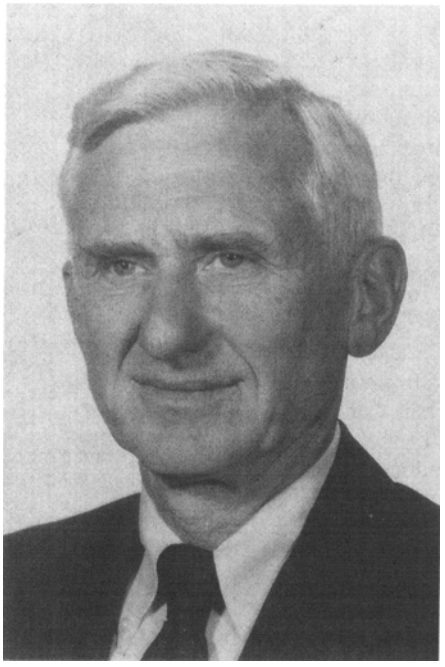

The Edward DeMille Campbell Memorial Lecture was established in 1926 as an annual lecture in memory of and in recognition of the outstanding scientific contributions to the metallurgical profession by a distinguished educator who was blind for all but two years of his professional life. It recognizes demonstrated ability in metallurgical science and engineering.

Merton C. Flemings received his S.B. degree from the Massachusetts Institute of Technology (MIT) in the Department of Metallurgy in 1951. He received his S.M. and Sc.D. degrees, also in Metallurgy, in 1952 and 1954, respectively. From 1954 to 1956, he was employed as Metallurgist at Abex Corporation, Mahwah, New Jersey, and in 1956 returned to MIT as Assistant Professor. He was appointed Associate Professor in 1961 and Professor in 1969. In 1970, he was appointed Abex Professor of Metallurgy. In 1975, he became Ford Professor of Engineering and, in 1981, Toyota Professor of Materials Processing. He initiated and became the first director of the Materials Processing Center in 1979, and in 1982, he became Head, Department of Materials Science and Engineering.

Professor Flemings is active in undergraduate and graduate teaching and research in materials science and engineering. He is a member of the National Academy of Engineering and of the American Academy of Arts and Science. He is author or co-author of 240 papers, 19 patents, and two books in the fields of solidification science and engineering, foundry technology, and materials processing. He received the Simpson Gold Medal from the American Foundrymen's Society in 1961 and the Mathewson Gold Medal TMS in 1969. In 1977, he was awarded the Henri Sainte-Claire Deville Medal by the Societe Francaise de Metallurgie. In October 1978, he received the Albert Sauveur Achievement Award from ASM INTERNATIONAL. In 1980, he received the John Chipman Award from AIME. In 1984, he was elected an honorary member of the Japan Foundrymen's Society and, in 1985, received the James Douglas Gold Medal from AIME. The Italian Metallurgical Association awarded him the Luigi Losana Gold Medal in 1986, and he was elected honorary member of The Japan Iron and Steel Institute of Japan in 1987. He was elected a TMS Fellow in 1989 and received the TMS Leadership Award in 1990.

Professor Flemings' research and teaching concentrate on engineering fundamentals of materials processing and on innovation of materials processing operations. He has worked closely with industry and industrial problems throughout his professional career. The focus of his current activities is the broadening and strengthening of the academic program of the Department of Materials Science and Engineering at MIT. In addition, he is active nationally in strengthening the field and in delineation of new directions for the field. He was co-chairman of a recently completed national study on Materials Science and Engineering, sponsored by the National Research Council, and he has recently completed a two-year chairmanship of the University Materials Council, a committee of heads of academic materials departments.

DURING dendritic solidification of castings and ingots, a number of processes take place simultaneously within the semisolid region. These include crystallization, solute redistribution, ripening, interdendritic fluid flow, and solid movement. The dendritic structure which forms is greatly affected by convection during the early stages of solidification. In the limit of vigorous convection and slow cooling, grains become spheroidal. Alloys with this microstructure possess rheological properties in the semisolid state which are quite different from those of dendritic alloys. They behave thixotropically, and viscosity can be varied over a wide range, depending on

processing conditions. The metal structure and its rheological properties are retained after solidification and partial remelting. The semisolid alloys can be formed in new ways, broadly termed "semisolid metal (SSM) forming processes." Some of these are now employed commercially to produce metal components and are also used to produce metal-matrix composites.

I. DENDRITIC SOLIDIFICATION

A. *The Liquid-Solid Zone*

Nearly all metal alloys of commercial importance solidify dendritically, either with a columnar or with an equiaxed dendritic structure, as illustrated in Figure 1. Solidification at rates typical of most castings and ingots is closely described by the simple model illustrated in Figure 2. Equilibrium very nearly pertains at liquid-solid interfaces, with negligible undercooling in front of the dendrite tips or between dendrite arms. The effect of curvature on the melting point is small, and except for special cases to be noted later, relative movement between liquid and solid can be neglected. Then, for a given temperature distribution in the solidifying casting (Figure 2(b)), the liquid composition at any location within the liquid-solid zone is defined by the liquidus line of the alloy system (Figure 2(c)). The fraction solid at a given location in the liquid-solid zone (Figure 1(d)) is given by a mass balance, which, in the simplest case, neglects ripening and diffusion in the solid.[1,2,3] For this case, the relation between weight fraction liquid in the liquid-solid zone, f_L, and liquid composition at a given location in the zone, C_L, is given by the Scheil equation, which may be written in the following form for constant partition ratio k:

$$f_L = \left(\frac{C_L}{C_0}\right)^{-1/1-k} \qquad [1]$$

where C_0 is initial composition. Since temperature, T, in the liquid-solid zone and C_L are related by the equilibrium liquidus line, Eq. [1] may also be written

$$f_L = \phi^{-1/1-k} \qquad [2]$$

where ϕ is dimensionless temperature $(T_M - T)/(T_M - T_L)$ and T_M and T_L are the melting point of the pure solvent and liquidus temperature of the alloy of composition C_0, respectively. Equation [2] illustrates the direct relationship of local weight fraction solid to temperature in the liquid-solid zone. It is often employed in experimental studies to calculate directly the local fraction solid from temperature measurements. The relationship is also often employed in mathematical models of solidification processes.

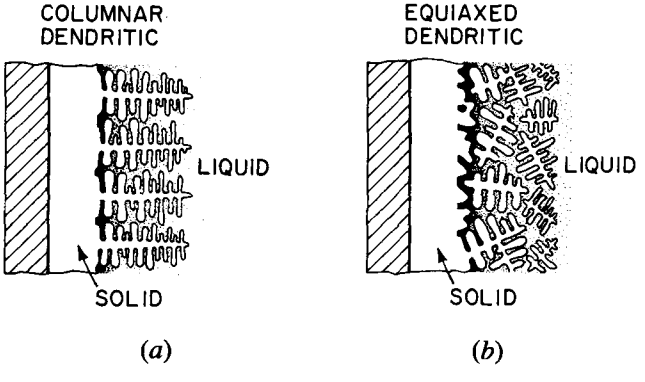

Fig. 1—Solidification of an alloy against a cold chill wall:[3] (*a*) columnar solidification and (*b*) equiaxed solidification.

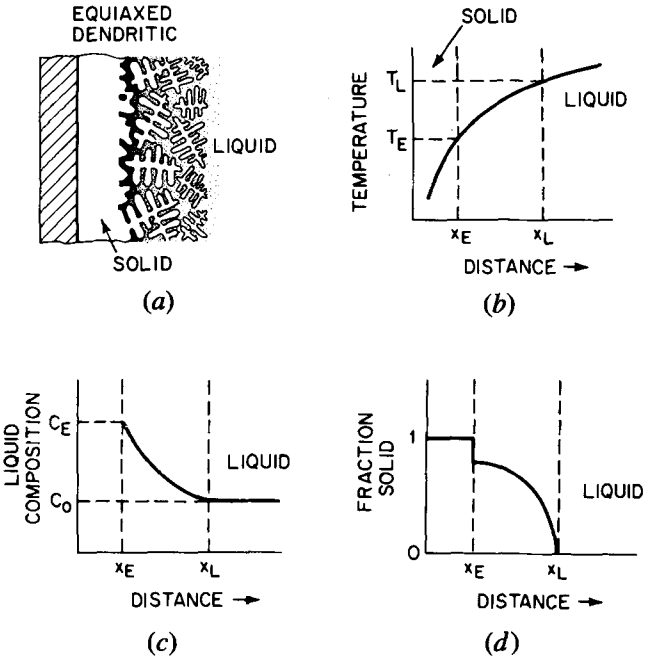

Fig. 2—Model of equiaxed solidification:[3] (*a*) dendrite structure; (*b*) temperature *vs* distance; (*c*) liquid composition *vs* distance; and (*d*) fraction solid *vs* distance.

Refinements of the Scheil equation are used to calculate local fraction solid with greater precision. For example, both diffusion in the solid and ripening occur to some extent in metal alloys during solidification, resulting in a somewhat higher fraction solid at a given temperature than that calculated from Eq. [2]. This problem has been treated by many researchers over the last 20 years, usually with the aim of calculating final microsegregation.[4–15]

The effect of ripening on fraction solid during solidification appears usually to be small, but the effects of solid diffusion can be significant. Figure 3 shows calculated fraction solid *vs* temperature for the model alloy Al-4.5 wt pct Cu for (a) no solid diffusion (*i.e.*, the Scheil equation), (b) a cooling rate of 1 Ks^{-1}, (c) a cooling rate of 0.01 Ks^{-1}, and (d) complete solid diffusion. Diffusion in the solid increases with decreasing solidification rate, but the increase is relatively small, since the longer time available for diffusion is partially counteracted by the larger diffusion distance (larger dendrite arm spacing).

For this alloy, diffusion in the solid is found to be negligible at cooling rates above about 2 to 5 Ks^{-1}, as illustrated by Figure 3 and first shown experimentally by Michael and Bever.[16] At these and higher cooling rates, however, another effect begins to have its influence on the relation between fraction solid and temperature: the dendrite tip temperature begins to drop below the liquidus temperature. That is, "dendrite tip undercooling" begins to become significant as a result of effects of tip

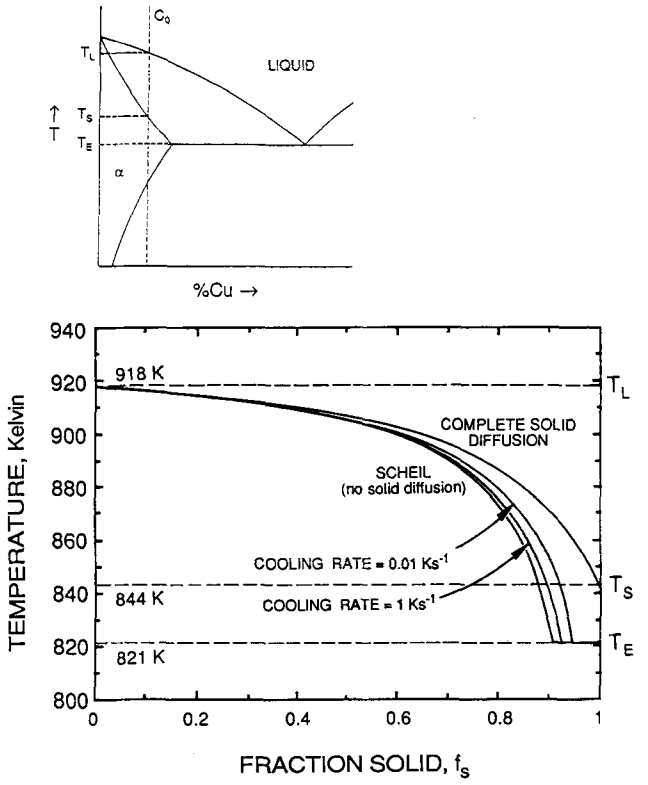

Fig. 3—Effect of diffusion in the solid on fraction solid *vs* temperature, Al-4.5 wt pct Cu alloy. Calculated curves for the limits of no solid diffusion and complete solid diffusion and for two intermediate cooling rates, based on the model of Brody and Flemings.[2] Schematic phase diagram is shown at upper left.

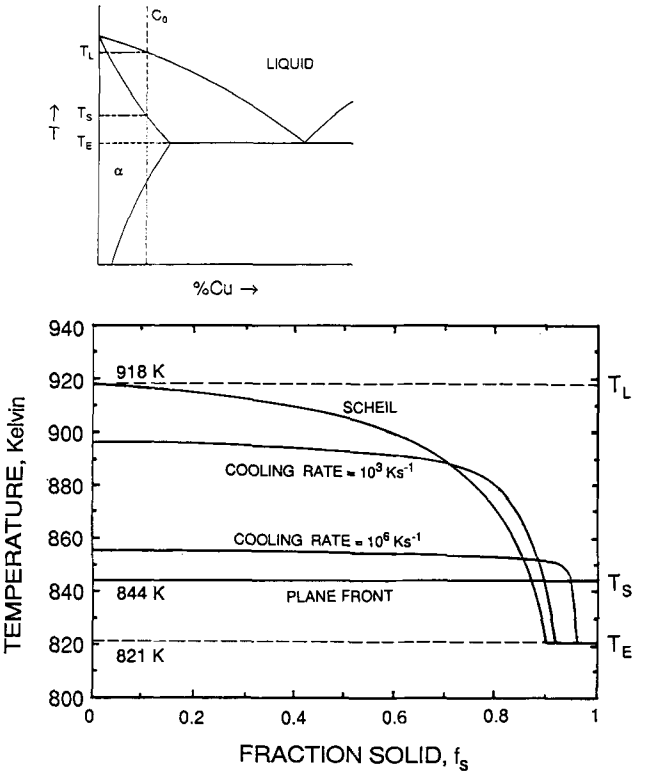

Fig. 4—Effect of dendrite tip undercooling on fraction solid *vs* temperature for columnar solidification of Al-4.5 wt pct Cu alloy. Calculations are based on the models of Kurz and co-workers[17,18] with the heat flow model of Campagna.[19,20] Columnar growth is assumed.

curvature and solute rejection, and at sufficiently high tip velocities, kinetic effects may also become important. Figure 4 shows calculations of the effect for Al-4.5 wt pct Cu alloy. Calculations are for fraction solid *vs* temperature, using the model of Kurz *et al.*[17] with equilibrium partition ratio to describe processes at the dendrite tip. The method of Giovanola and Kurz[18] is then used to "patch" the tip solution to the Scheil equation. Solution requires a relationship between cooling rate and tip velocity, and this is done using the heat flow model of Campagna,[19,20] assuming columnar dendrite growth. In the case of equiaxed solidification, deviation from the Scheil equation would be much less than that of Figure 4, because repetitive nucleation reduces the velocity of any dendrite tip.

B. *Dendrite Morphology*

In both equiaxed and columnar structures, the dendrites themselves evolve greatly during solidification, as a result of ripening due to surface energy.[3,9,21] Figure 5 shows this schematically. The structure becomes gradually coarser during solidification as a result of the remelting of dendrite arms of smaller radius. The parameter usually chosen to measure this change is secondary dendrite arm spacing, d. In accordance with expected ripening kinetics, it is found that final dendrite arm spacing bears an approximately cube-root relationship to the "local solidification time" or, inversely, to the cooling rate (Figure 6).[22]

The increase of dendrite arm spacing takes place only during the initial portion of the solidification time. In later stages of solidification (perhaps above about f_s = 0.5), liquid-solid surface area can be most effectively reduced by the filling of spaces between rodlike arms to form plates; such plates are commonly observed in alloys which solidify without too high a fraction eutectic (Figure 7).[23]

C. *Deformation Behavior of Semisolid Dendrites*

When a casting of equiaxed grains solidifies in "mushy" fashion, as illustrated in Figure 8, the top surface of the casting can be seen to settle more or less uniformly in the early stages of solidification. Early in solidification, the grains are free to move (to "settle"). At some critical local solid fraction, the grains form a network, and this stage of "mass feeding" ceases. The fraction solid at which the dendrites form a cohesive network, and at which the network begins to develop some strength, depends on dendrite size and morphology, but a number of studies in different alloys show it to be in the range of about 0.1 to 0.2 and occasionally higher. As one example, Metz and Flemings[24] isothermally sheared small blocks of aluminum alloys and found negligible strength below about 0.2 fraction solid.[24,25] Above 0.2 fraction solid, shear strength increased with increasing fraction solid (Figure 9). Shear strength was found also to increase somewhat with increasing strain rate and with increasing grain size. In well grain-refined alloys, strength did not begin to develop until 0.4 fraction solid.

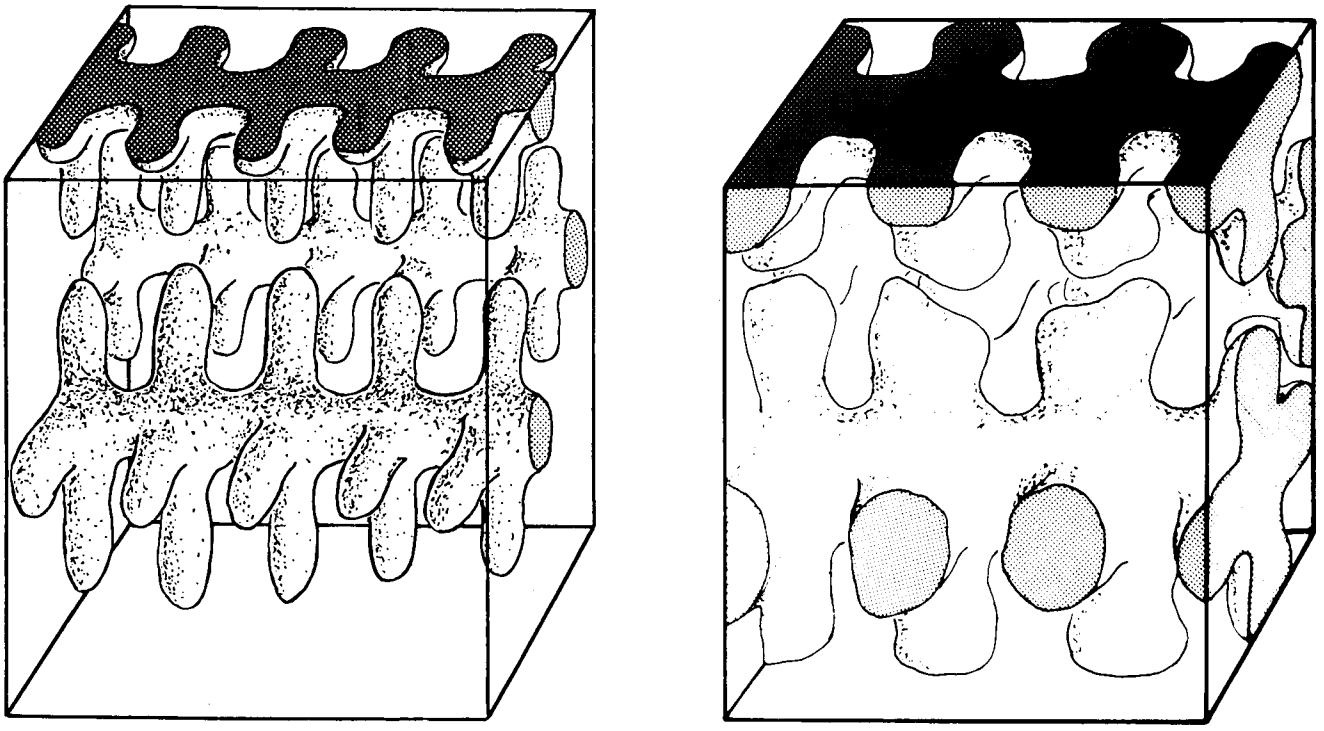

(*a*) (*b*)

Fig. 5—Schematic illustration of ripening. Dendrite structure shown (*a*) early in solidification and (*b*) at about 50 pct solid.

Spencer *et al.*[26] carried out similar tests on Sn-15 pct Pb alloy. Their test apparatus consisted of two grooved counter-rotating cylinders (Figure 10). Maximum stresses obtained in the tests were qualitatively similar to the results of Metz and Flemings[25] on aluminum alloys. Measurable strength began to develop at a fraction solid of about 0.2.

Typical isothermal stress-strain curves for Spencer *et al.*'s semisolid alloy[26] are shown in Figure 11. At a given strain rate, stress increases with displacement to a maximum, after which it falls to a low value. Maximum strength increases with increasing fraction solid. Deformation at fractions solid up to about 0.9 is primarily by grain-boundary sliding, with some dendrite distortion, as shown by the microstructure at the upper right of Figure 11. Some bending of dendrites is apparent, as are regions where spaces between grains have opened up and are filled with liquid. The increase of stress with initial strain is probably because strain increases the number of contacts (the "welds") between particles. At sufficiently high strain, continuous fissures open, so stress falls to a

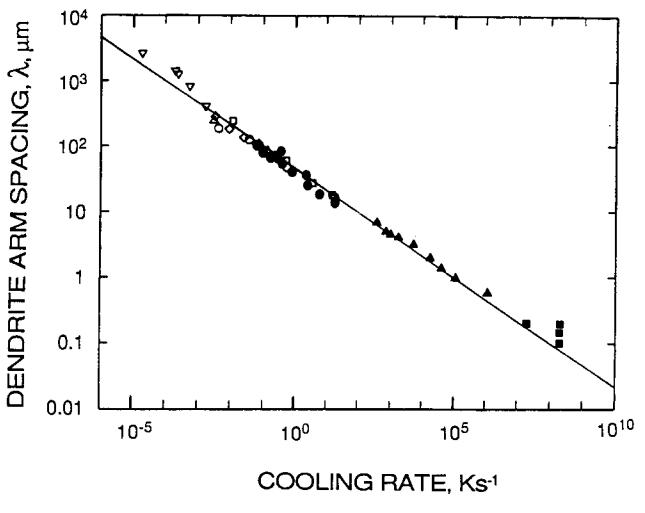

Fig. 6—Dendrite arm spacing *vs* cooling rate for alloys of Al-4.5 wt pct Cu. Experimental data are from a number of different investigators.[22]

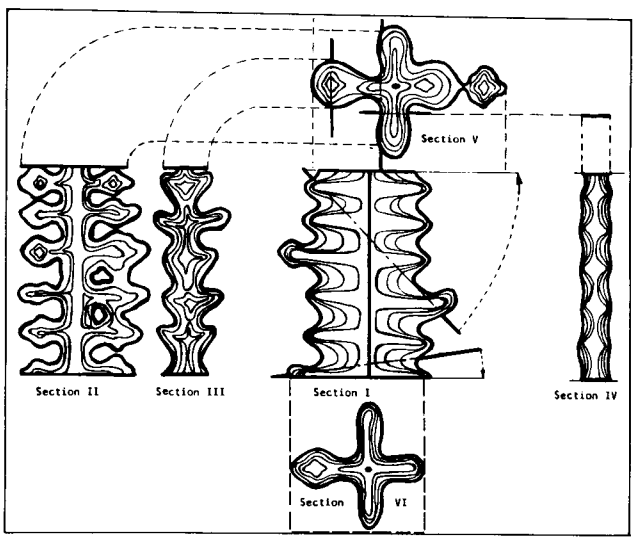

Fig. 7—Schematic illustration of infilling of dendrite arms to form dendrite plates in a low alloy steel.[23]

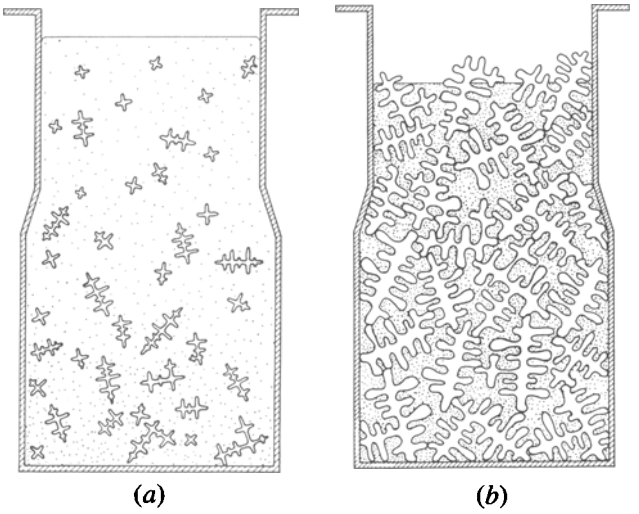

Fig. 8—Feeding of a mushy freezing alloy (schematic): (*a*) mass feeding stage and (*b*) interdendritic feeding stage.

low level. The fissures become filled with liquid except at very high fractions solid.

Strains such as the foregoing, with resulting liquid flow, result in localized regions of macrosegregation in actual castings and ingots. A common source of the strain is thermal contraction of the solidifying metal, hindered by mold constraint.[27,28] Figure 12 is an example of a local segregate in Al-4.5 pct Cu alloy; the segregates are sufficiently sharply defined that they are termed "filled hot tears." Centerline segregation in continuous casting can be visualized as having a similar root cause, resulting from thermal contraction of the solid, accentuated by "bulging" of the casting due to metallostatic head.[29] Detailed analysis of compositional variations across a casting cross section such as this requires analysis of the

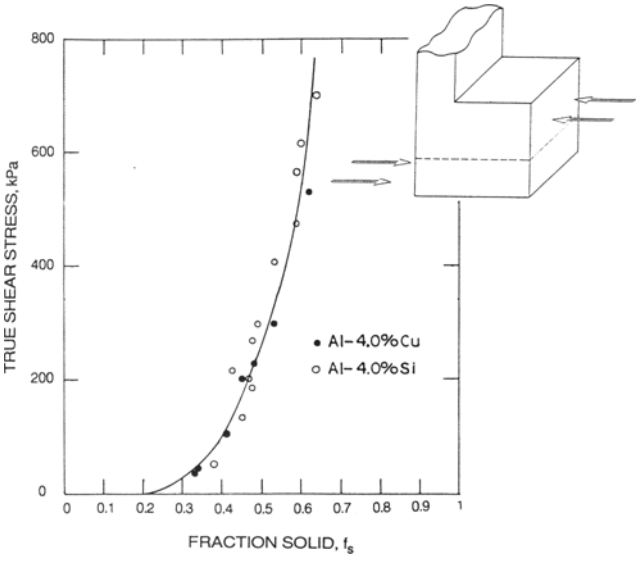

Fig. 9—Isothermal shear strength of semisolid dendritic aluminum alloys. Shear stress plotted is that after a small amount of shear (6.25-mm shear at a strain rate of 0.049 mm s^{-1}). Schematic at upper right shows test specimen.[25]

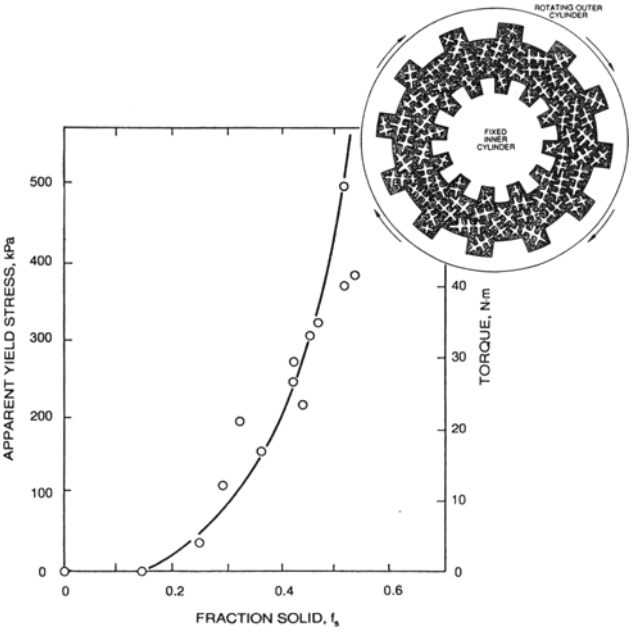

Fig. 10—Isothermal shear strength of semisolid dendritic Sn-15 wt pct Pb alloy. Shear stress is the maximum measured (at a shear rate of 0.16 s^{-1}). Schematic at upper right shows test arrangement.[26]

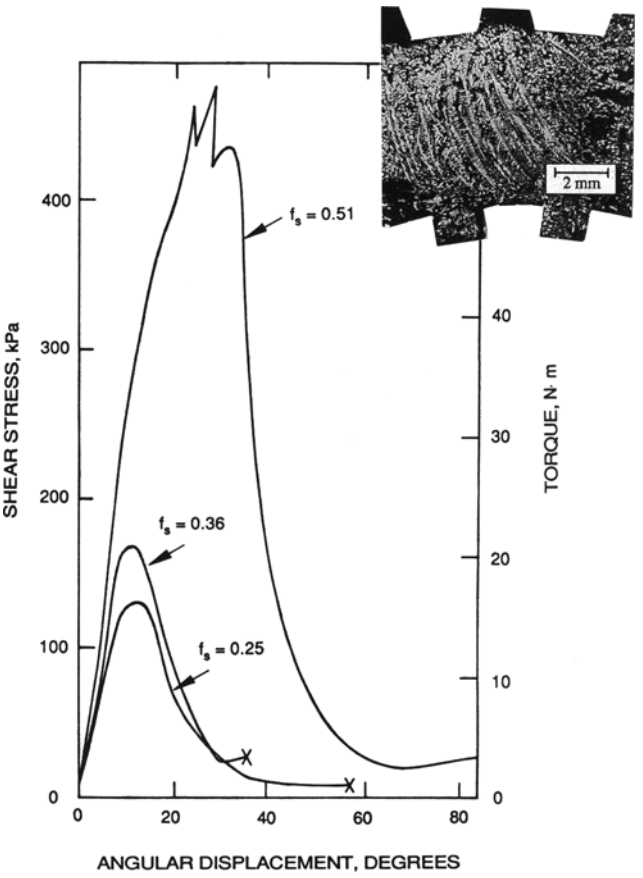

Fig. 11—Isothermal shear test results of semisolid Sn-15 pct Pb alloy. Photograph at upper right shows actual specimen macrostructure.[26]

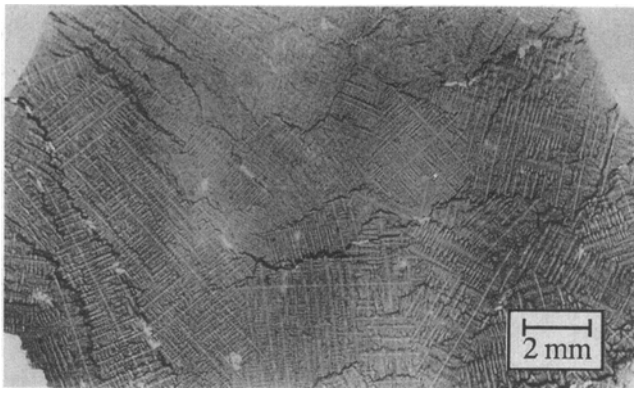

Fig. 12—Thin section radiograph of a section of an Al-10 pct Cu alloy casting with "filled hot tears."[27]

full thermal and interdendritic flow fields during solidification.[3,30] Figure 13 is an example.

At sufficiently high solid fractions (above about f_s = 0.9), liquid can no longer flow to compensate for thermal or other strains in the solidifying metal. Then, if stresses are large enough to overcome the strength of the partially solid material, internal or open "hot tears" result. Figure 14 shows an example of a hot tear test casting employed by foundrymen. When the casting is sufficiently long and the mold is sufficiently rigid, the casting tears apart during solidification. Hot tear susceptibility is strongly alloy-sensitive. Alloys most prone to hot tearing are those which solidify over a wide temperature range but with a relatively small amount of residual liquid at the eutectic temperature.[27,28] As shown

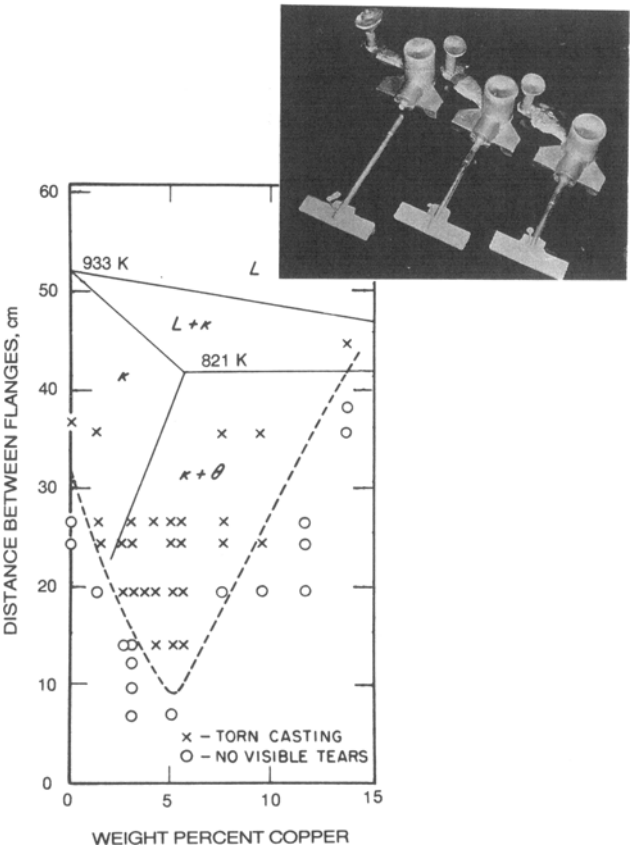

Fig. 14—Hot tear testing of Al-Cu alloy. Plot shows maximum length test casting that can be made without visible tears. Photograph at upper right shows actual test specimens of Al-4.5 wt pct Cu alloy.[27]

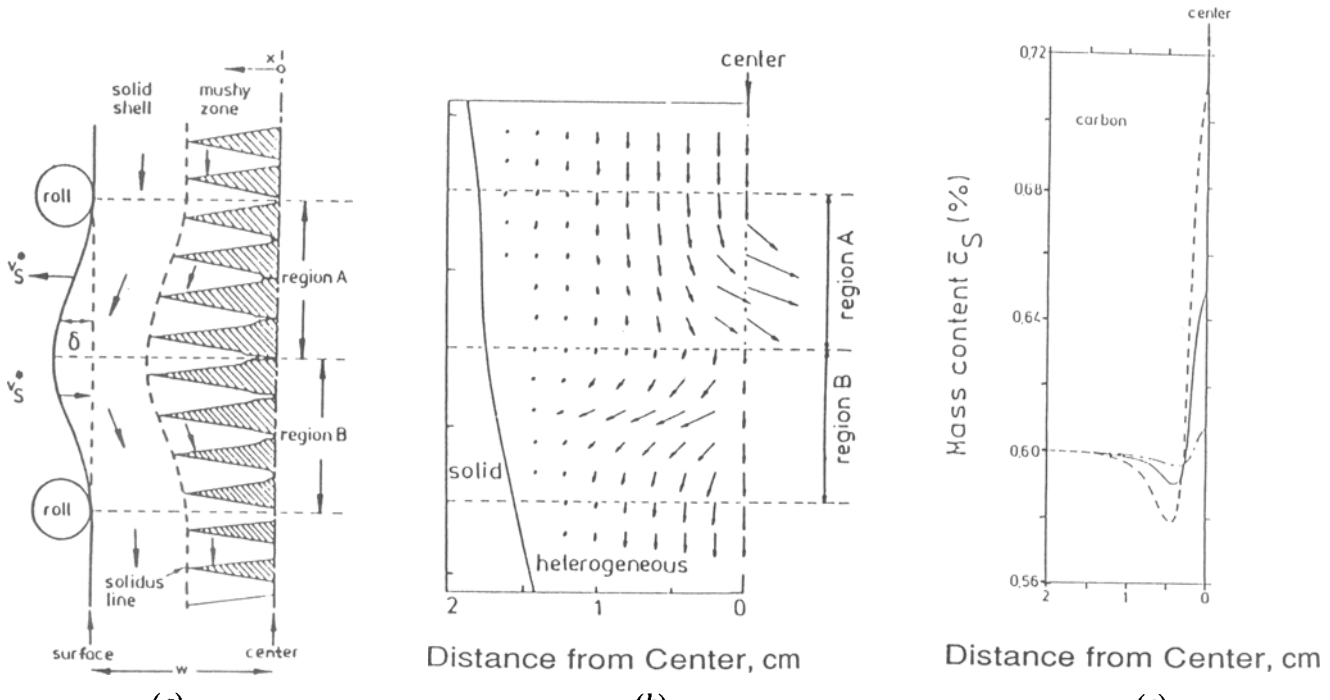

Fig. 13—Centerline segregation due to "bulging" in continuous casting:[29] (*a*) schematic of physical model, (*b*) interdendritic flow lines, and (*c*) resulting macrosegregation.

in Figure 14, greatest hot tear susceptibility in Al-Cu alloys is at about 5 wt pct Cu.

D. *Grain Size*

Columnar grains in castings and ingots may be many centimeters long. Their diameter may range from less than 0.1 mm to 1 cm or more. Generally, the diameter of columnar grains increases progressively as solidification proceeds, since those grains which have a preferred growth direction oriented near the heat flow direction tend to "crowd out" less favorably oriented grains.

Equiaxed grains typically also range in size from less than 0.1 mm to over 1 cm. Effective grain refiners (heterogeneous nucleating agents) are available for most nonferrous alloys. Through the use of these, it is possible, in practice (especially with aluminum and magnesium alloys), to obtain grain sizes consistently under about 0.1 mm. Grain refiners have been developed for ferrous and nickel-base alloys which are effective as mold coatings for thin-section castings, but their effective life is not sufficiently long for refinement of sections more than a few millimeters thick.[3] To achieve smaller grain sizes than can be achieved with available grain refiners, and especially to refine grain size of metals for which grain refiners are not available, we need to turn to other methods.

Vibration (ultrasonic and sonic) has been shown to influence formation of new grains, and there has been much speculation as to the mechanism for this. An interpretation favored by many some decades ago was that the vibration promoted heterogeneous or even homogeneous nucleation.[31] Others[32] were inclined to the earlier explanation of Schmid and Roll[33] that the grain refinement derived from fragmentation of primary crystallites, providing an artificial source of more nuclei. This latter one is the prevalent view today.

Foundrymen and ingot casters have long understood that equiaxed grains are favored over columnar grains by low pouring temperature (low "superheat"). As pouring temperature is lowered further, the equiaxed grains become finer. We now understand that the major cause of the foregoing is convection at low pouring temperature: the convection associated with the mold filling itself remains strong as solidification commences. With high pouring temperatures, on the other hand, the forced convection dissipates before solidification begins, so that solidification proceeds in a relatively quiescent melt. Columnar grains (or large equiaxed grains) are favored at a given pouring temperature when convection is minimized by application of a magnetic field[34] or by casting in a thin section within which convection is quickly dissipated.[35]

More importantly from a practical standpoint, introducing convection by mechanical or electromagnetic means during the early stages of solidification favors formation of fine, equiaxed grains. There are many references in the older cast metals literature as to the effect of such convection on grain structure. Mold oscillation, for example, was sometimes employed to achieve fine grains in sand castings, and stirring with a cold rod was used to refine the structure of ingots. Today, electromagnetic stirring is widely practiced in continuous casting to achieve fine grain size.

There is general belief today that vibration, low pouring temperature, and externally induced convection all promote grain refinement primarily by a dendrite fragmentation mechanism, although there is not yet agreement on what that basic mechanism is. Some possible dendrite fragmentation mechanisms are

(a) Dendrite arm fracture, in which arms shear off as a result of the force on the arm from the fluid flow.[36,37]
(b) Remelting of the arm at its root as a result of normal ripening.[21] The function of the fluid flow in this case is to alter or accelerate the solute diffusion involved in ripening and to carry the dendrite arm away from its "mother grain" to where it can grow as a new grain.
(c) Remelting as above, enhanced by thermal perturbations which result from turbulent convection.
(d) Remelting as above, but where the melting at the root is accelerated by the stress introduced at the dendrite root as a result of the force of the fluid flow.
(e) As in (c) above, but where the melting at the root is further enhanced by a high solute content in the solid at the dendrite root.[34]
(f) Recrystallization as a result of the stress introduced by the force of the fluid flow, with rapid liquid penetration along the new grain boundaries.[38,39]

II. NONDENDRITIC SOLIDIFICATION

A. *Semisolid Slurries*

During the course of his doctoral thesis research in early 1971, Spencer was conducting the hot tearing tests on Sn-15 pct Pb alloy discussed earlier (Figures 10 and 11).[40] In the course of those experiments, he decided to use the same apparatus to conduct a quite different type of test. Instead of partially solidifying the alloy before beginning shear, he began the shear above the liquidus and then slowly cooled his alloy into the solidification range while it was being sheared.

The results were surprising. Shear stress increased only very slowly as temperature was decreased below the liquidus. The stress measured at a given temperature below the liquidus was orders of magnitude less than when the samples were cooled to the given temperature before shear. Comparison of Figures 10 and 15 shows this remarkable reduction in shear stress. For example, in the dendritic material, maximum shear stress at a little over $f_s = 0.4$ is 200 kPa. In the nondendritic material at the same fraction solid, it is three orders of magnitude less, 0.2 kPa. In both of these figures, fraction solid, f_s, is calculated from the Scheil equation based on actual temperature measurements.

The grain structure obtained in these early experiments was nondendritic, as shown schematically by the inset in Figure 15, and it was evident that shearing in the material was taking place more or less uniformly throughout the sample. The material was behaving as a liquidlike slurry, to which an apparent viscosity could be assigned, as has been done in Figure 15.[26,40] Note that the viscosities are quite low at a fraction solid of 0.4; for example, viscosity is less than that of olive oil (less than 1 Pa · s).

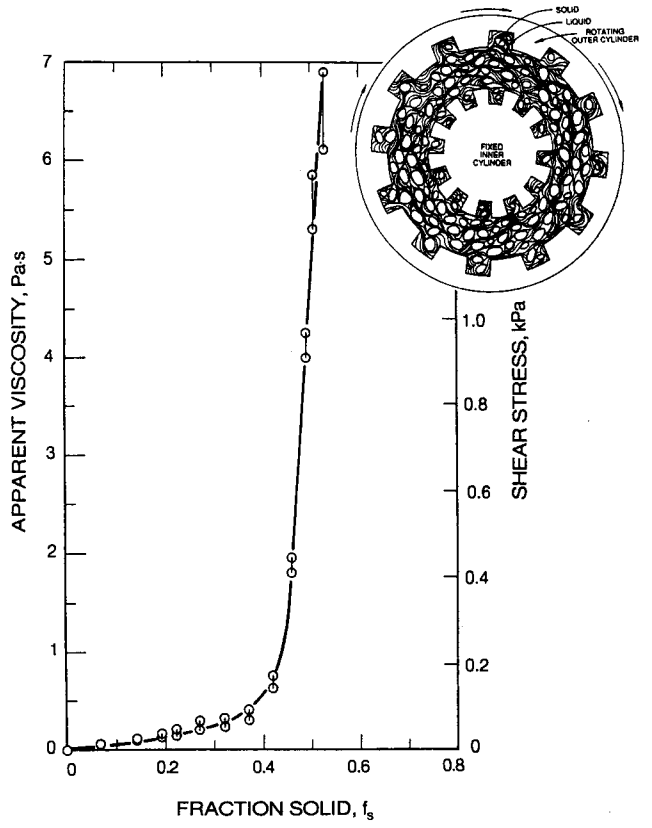

Fig. 15—The Spencer experiment.[26] Experimentally determined viscosity and shear stress *vs* fraction solid for Sn-15 wt pct Pb alloy cooled at 0.006 Ks^{-1} with a shear rate of 200 s^{-1}. Schematic at upper right is an illustration of the test specimen.

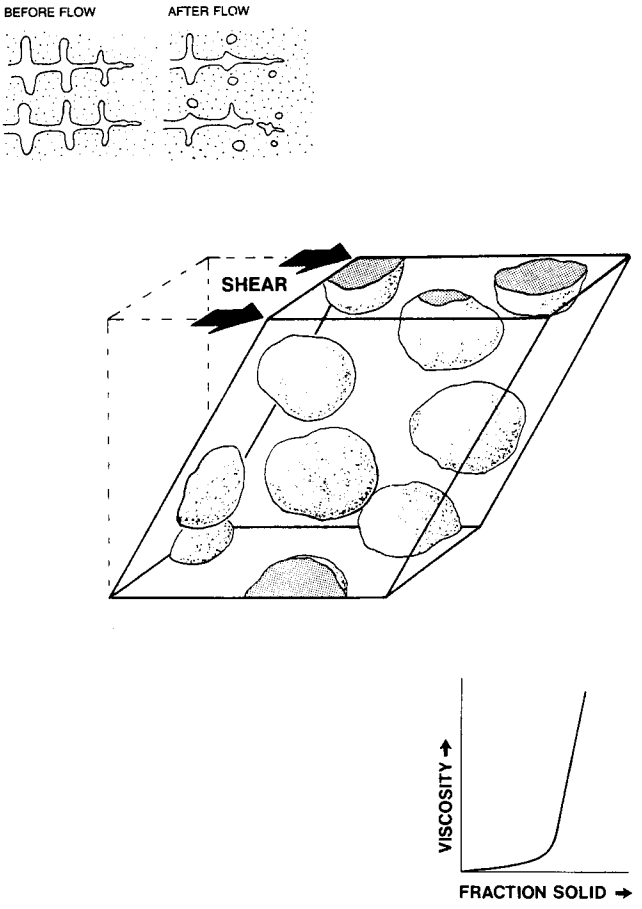

Fig. 16—Fundamentals of semisolid forming. Top left: breaking of dendrite by shear; center: rheological behavior of a volume element of semisolid nondendritic material; bottom right: viscosity *vs* fraction solid.

Structure and flow behavior is further illustrated schematically in Figure 16. We came, in our early work at MIT, to call the process of obtaining these new structures "rheocasting," to signify the distinctive rheological behavior of the material. Today, this process and related processes to be discussed below are often grouped under the term "semisolid metal (SSM) forming."

In the nearly 20 years that have now elapsed since the initial discovery of Spencer,[40] many studies have been conducted on fundamental and engineering aspects of vigorously agitated SSM's. Nonetheless, there is still much that is not understood in detail about the mechanisms of structure formation or about the rheology of the material. In the following paragraphs, a selective review is given of results of basic studies conducted over the last two decades. In the course of the discussion, mechanisms of structure formation and of rheological behavior are described which seem to fit the observed results. However, the reader is cautioned that the mechanisms given are, for the most part, qualitative, may not be fully correct, and may not be fully general.

Vigorous agitation, as solidification begins, results in formation of new grains by one or another of the mechanisms described in the previous section (Figure 17(a)). The early growth of each dendrite fragment then continues dendritically, as shown schematically in Figure 17(b). With continuing shear and time during solidification, the dendrite morphology becomes that of a "rosette" (Figure 17(c)), as a result of ripening, shear, and abrasion with other grains. Ripening proceeds during further cooling (Figure 17(d)). With sufficiently slow cooling and high shear, the particles become spheroidal (or, in some cases, ellipsoidal), usually with a small amount of entrapped liquid, as shown in Figure 17(e). The extent to which the morphology evolves along the spectrum from that of Figure 17(a) to that of Figure 17(e) increases with increasing shear rate and amount of solidification and with decreasing cooling rate. The size of the individual grains (dendrites or rosettes) appears to depend only moderately on shear rate above some given minimum value but depends strongly on cooling rate—at least the cooling rate during the initial stages of solidification.

Some examples of structural changes in actual rheocast materials are shown in Figures 18 through 20. Figure 18 shows three structures from Spencer's original work.[40] All three samples were cooled continuously to a given fraction solid and then water-quenched. In Figure 18(a), a low shear rate of 20 s^{-1} was employed, and the sample was quenched when it was only 0.35 fraction solid. The structure is seen to be quite dendritic. When, however, cooling was continued at the same shear rate to $f_s = 0.5$, the structure became quite spheroidal, although with considerable entrapped or semientrapped liquid (Figure 18(b)). A higher shear rate of 200 s^{-1} resulted in a similar structure but with less entrapped liquid (Figure 18(c)).

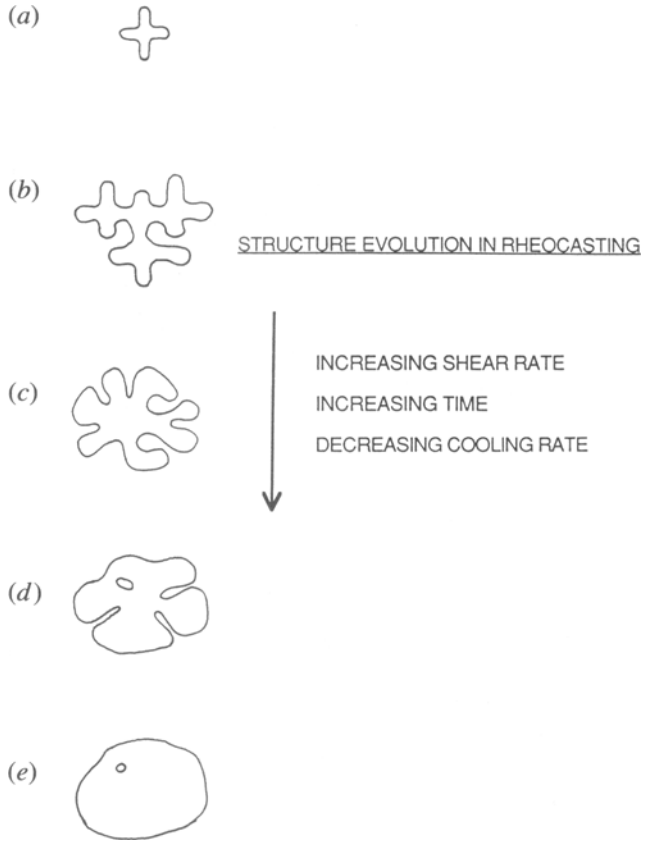

Fig. 17—Schematic illustration of evolution of structure during solidification with vigorous agitation: (*a*) initial dendritic fragment, (*b*) dendritic growth, (*c*) rosette, (*d*) ripened rosette, and (*e*) spheroid.

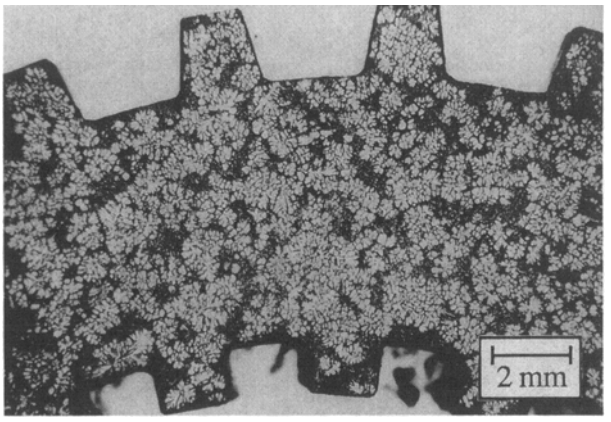

(*a*)

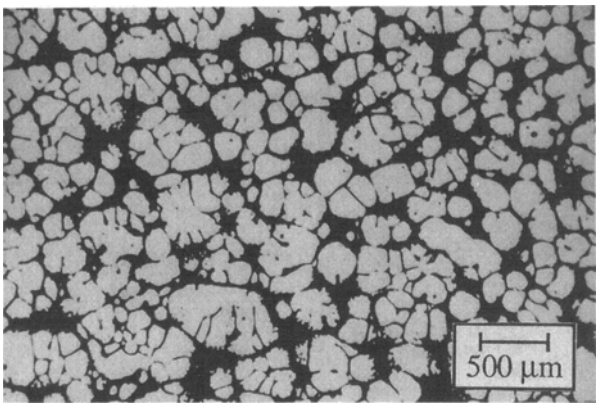

(*b*)

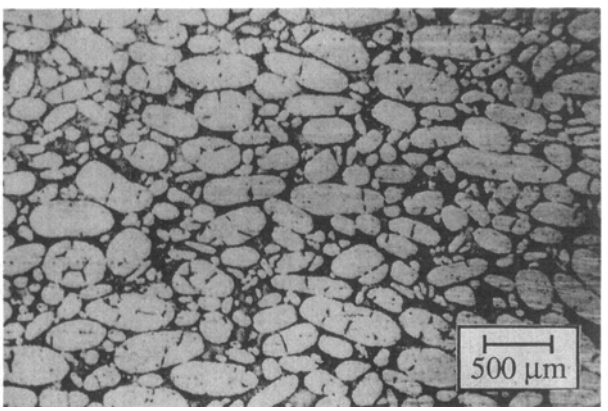

(*c*)

Fig. 18—Sn-15 wt pct Pb alloy continuously cooled at 0.006 Ks^{-1}: (*a*) low shear rate and low fraction solid (shear rate 20 s^{-1}, cooled to f_s = 0.35 and then quenched); (*b*) cooled at low shear rate (20 s^{-1}) to f_s = 0.5 and then water quenched; and (*c*) cooled at high shear rate (200 s^{-1}) to f_s = 0.5 and then water quenched.

Structure evolution toward more spheroidal (or ellipsoidal), dense, primary particles continues when the semisolid slurry is sheared isothermally. Figure 19 is an example from thesis work of Joly, who continued Spencer's studies using the same alloy and equipment.[41,42] Joly found reduction of entrapped liquid over isothermal shearing times of up to 5400 seconds. Similar structures are seen in Figure 20 for rheocast Al-6.5 wt pct Si from recent thesis research of Moon.[43]

Primary grain size (particle size) in these sheared structures is strongly influenced by cooling rate (Figure 21).[44] Particle diameter at a given cooling rate tends to be about equal to what the primary dendrite arm spacing would be in an unstirred melt, suggesting that the frequency of dendrite fragmentation is related to the number of growing primary arms in a solidification front.

B. *Effect of Shear Rate and Cooling Rate; Pseudoplastic and Thixotropic Behavior*

When viscosity of a semisolid metal slurry is measured during continuous cooling, it is found to be a strong function of shear rate, decreasing with increasing shear rate, as shown in the two examples in Figure 22. Viscosity is also strongly dependent on cooling rate, as illustrated by the two examples in Figure 23. These two effects can be understood, in part, in terms of the irreversible structural evolution sketched in Figure 17. Both increasing shear rate and decreasing cooling rate result in denser, more rounded particles which move more easily past one another.[26,42,45–59]

As will be seen, however, these irreversible structural changes cannot fully explain the dependence of viscosity on shear rate. There is another effect, characteristic of many liquid-solid slurries. That is that a larger scale

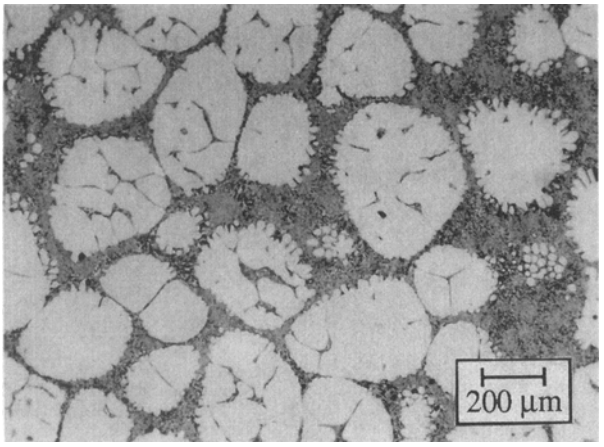

(*a*)

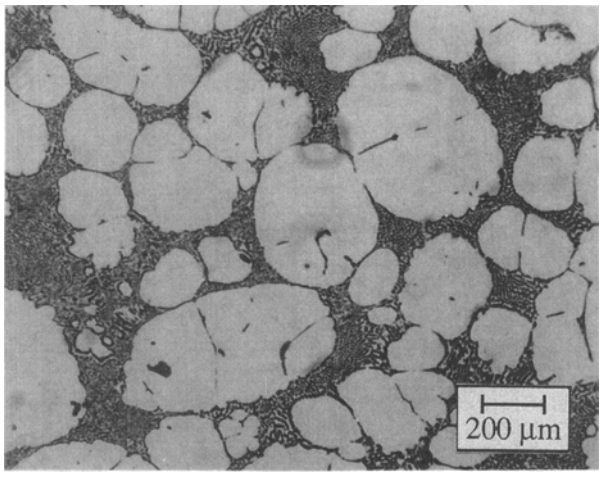

(*b*)

Fig. 19—Structure evolution in Sn-15 wt pct Pb alloy, isothermally sheared at a rate of 230 s^{-1} with 0.45 fraction solid: (*a*) 730 s and (*b*) 2400 s.[41]

"structure" builds by collision and coalescence of favorably oriented particles, as sketched in Figure 24.[60] The extent of this larger structure, and hence, the viscosity, depends on a balance between the rate of structure buildup and its breakdown from shear. We expect this structure buildup and breakdown to be more or less reversible with changing shear rate.

In rheological terms, these semisolid slurries are said to exhibit "pseudoplasticity." Empirical equations developed to describe the full range of viscosity of pseudoplastic materials require at least four parameters. However, a simple and widely used relation that is often useful over wide ranges of shear rate is the well-known "power-law" model:

$$\eta = K\dot{\gamma}^{n-1} \qquad [3]$$

where η is viscosity, $\dot{\gamma}$ is shear rate, n is called the "power-law index," and K is the "consistency." The smaller the power-law index, the greater the pseudoplasticity. We may use this simple model to help understand the effects of process variables on viscosity of semisolid alloys.

Figure 25 plots results from recent thesis work at MIT

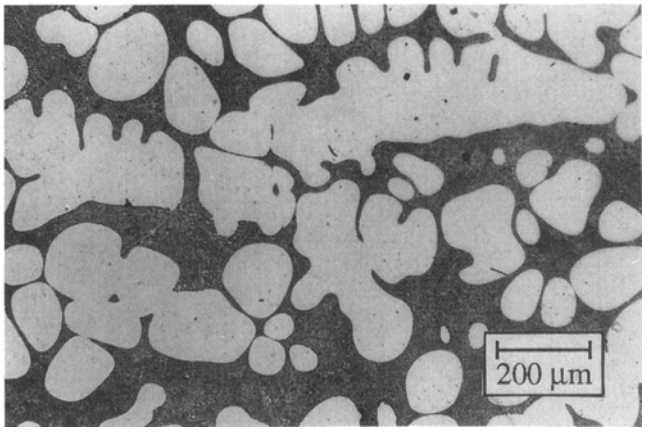

(*a*)

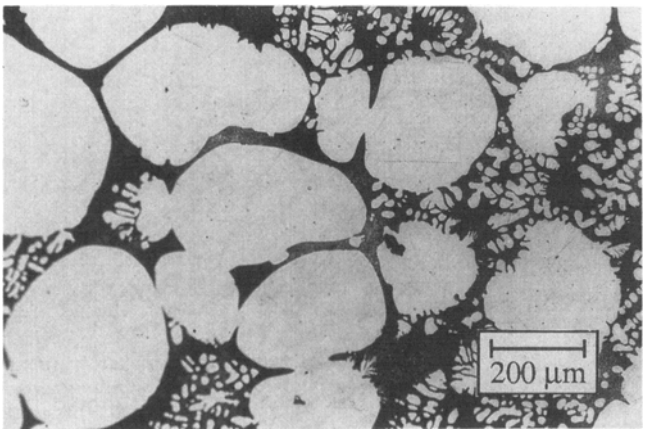

(*b*)

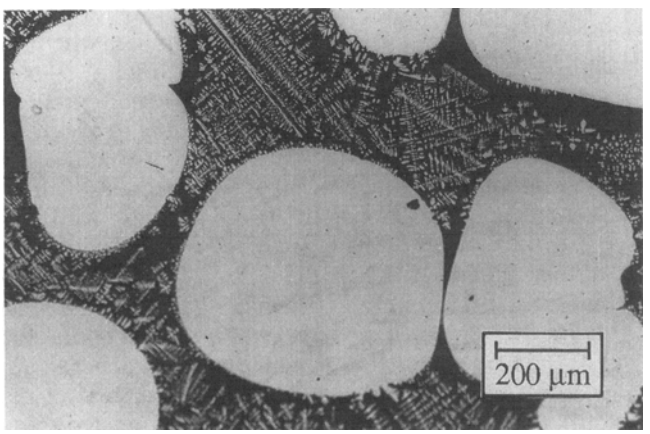

(*c*)

Fig. 20—Structure evolution in Al-6.5 wt pct Si alloy:[43] (*a*) Continuously cooled at 0.075 Ks^{-1} shear rate to 0.52 fraction solid; (*b*) isothermally sheared at 180 s^{-1} and 0.4 fraction solid for 2 h, and (*c*) same as (b) but with 24 h rest time after shearing.

by Moon on Al-6.5 wt pct Si alloy.[43] Viscosity is shown at 0.4 fraction solid as a function of shear rate for a number of different initial conditions. Note that viscosity at a given shear rate can vary by over an order of magnitude. Data for the top curve were obtained by cooling to $f_s = 0.4$ and recording the viscosity obtained immediately on reaching this fraction solid; cooling time from

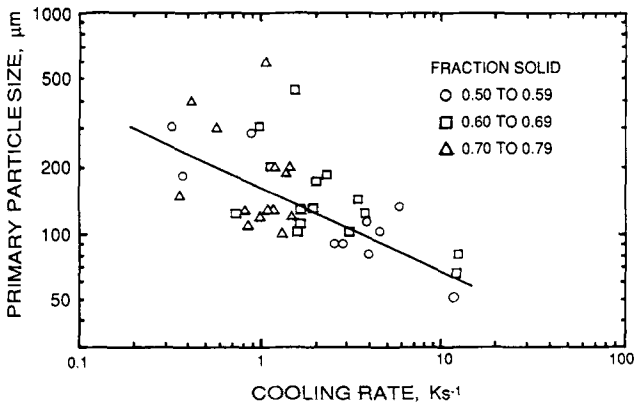

Fig. 21 — Primary particle size *vs* cooling rate, Sn-15 wt pct Pb alloy.[44]

the liquidus to this fraction solid was approximately 300 seconds. Viscosity is high at the low shear rates, partly because of the somewhat dendritic form of the grains and partly because of agglomeration of these grains as sketched. At higher shear rates, the agglomeration decreases, and the grains become more rosettelike.

The middle curve applies to data obtained either after very slow cooling or after extended isothermal holding at the given fraction solid. This curve is termed the "steady-state curve," since little change is observed in slower cooling or higher holding time. Here the grains are dense spheroids, with more agglomeration at the lower shear rates, as shown. The spheroidal grain structure at steady state results in a substantial drop in viscosity as compared with the material that is rapidly and continuously cooled.

Approximately reversible pseudoplastic behavior appears to be typical for "steady-state" curve experiments. That is, "structure" of the type illustrated in Figure 24 builds and is destroyed depending on shear rate. There is, however, a time dependency (thixotropy), so that when shear rate is abruptly changed, the new steady-state viscosity is attained only after some time at that shear rate. This effect is illustrated by the bottom curve of Figure 25, in which instantaneous viscosity is given after dropping the shear rate from 900 s^{-1} to the shear rate plotted. This instantaneous viscosity is less at any given shear rate than the "steady-state" value, because the "structure" has not had time to adjust to that of the new

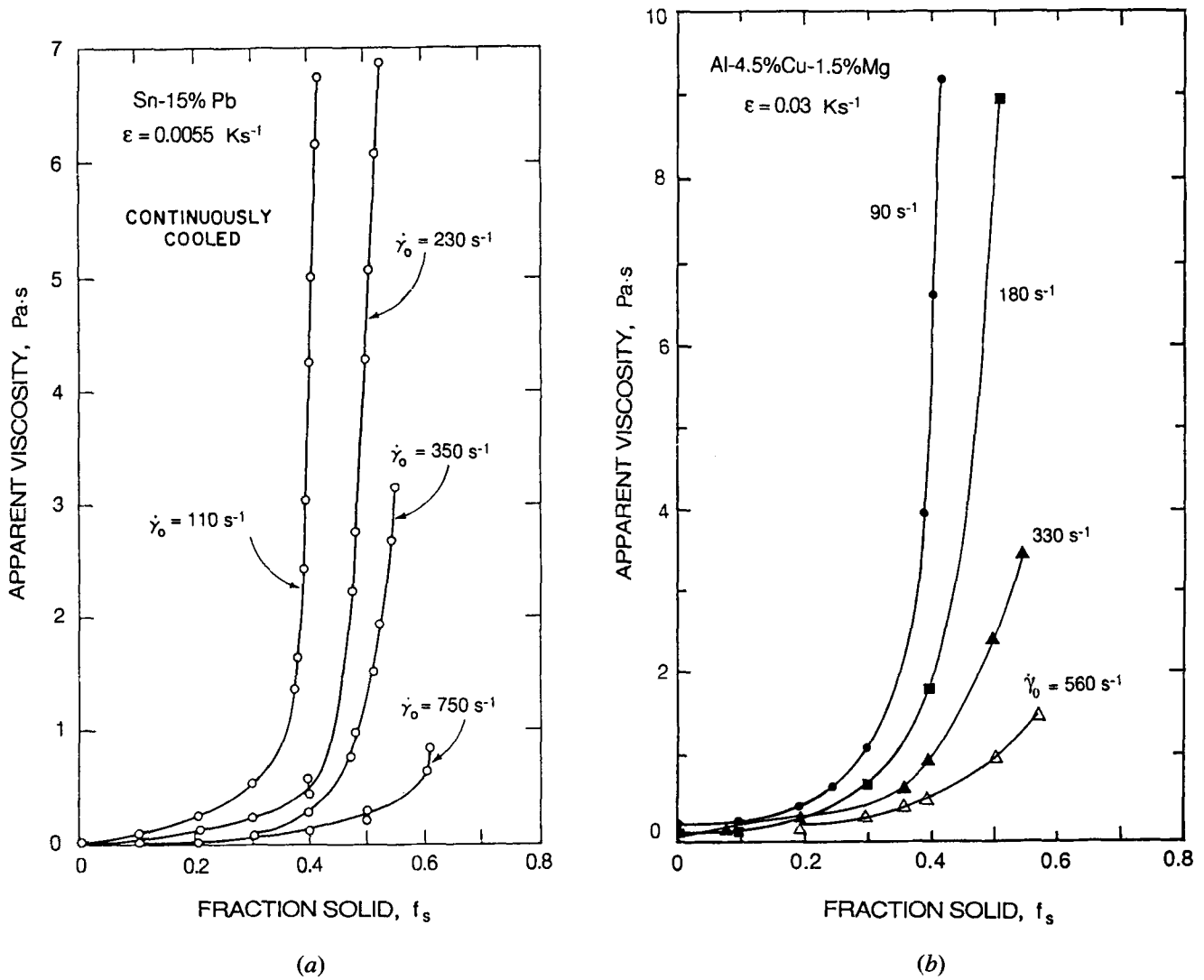

Fig. 22 — Effect of shear rate on apparent viscosity of semisolid alloys: (*a*) Sn-15 wt pct Pb[42] and (*b*) Al-4.5 pct Cu-1.5 wt pct Mg.[44]

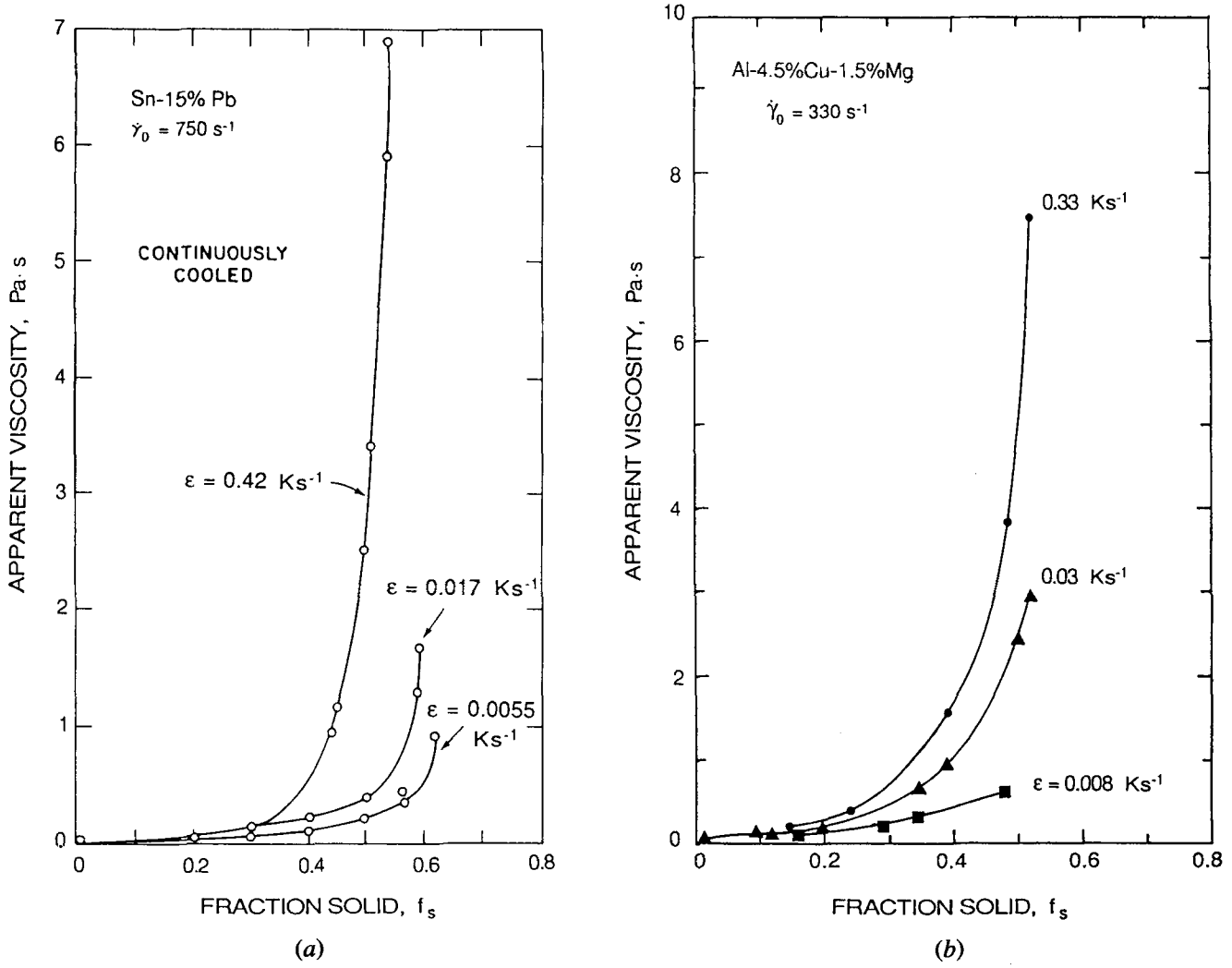

Fig. 23—Effect of cooling rate on apparent viscosity of semisolid alloys: (*a*) Sn-15 wt pct Pb[42] and (*b*) Al-4.5 wt pct Cu-1.5 pct Mg.[45]

shear rate. With time, agglomerates build, and the viscosity at a given shear rate approaches the steady-state value. The difference between this curve of "instantaneous viscosity" and the steady-state curve is a measure of the thixotropy of the slurry.

Figure 26 shows another measure of the thixotropic effect. In this example, specimens of the same alloy as above were brought to the steady-state viscosity of 0.06 Pa·s at $\dot{\gamma} = 900\ s^{-1}$. Shearing was then stopped for varying times up to 5000 seconds and then restarted at the same rate. Instantaneous viscosity is much higher at the start of shear, reflecting the "structure" that builds up during the rest. With time, viscosity decreases to about the steady-state value as the structure breaks down. Only quite short times are required for this breakdown to take place, whereas the structural buildup requires much longer times.

Still another way to measure extent of the thixotropy

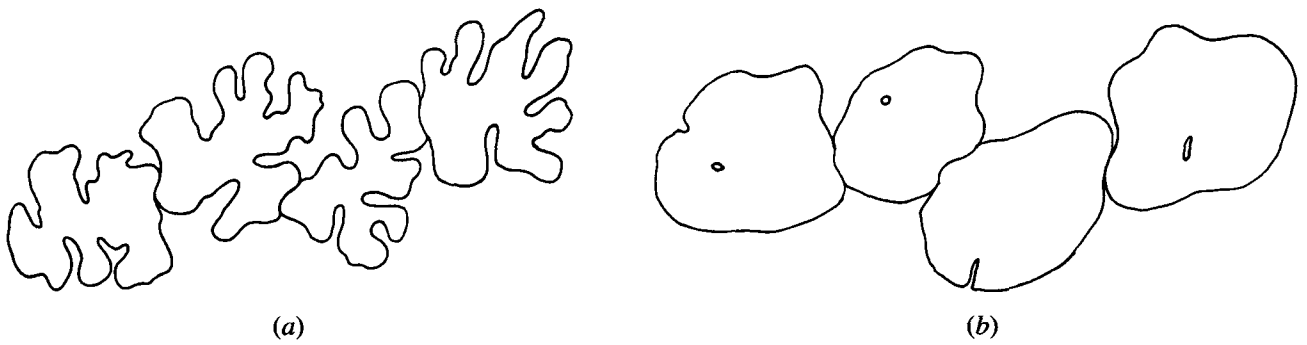

Fig. 24—"Structure" buildup from collision and coalescence: (*a*) rosettes and (*b*) spheroids.

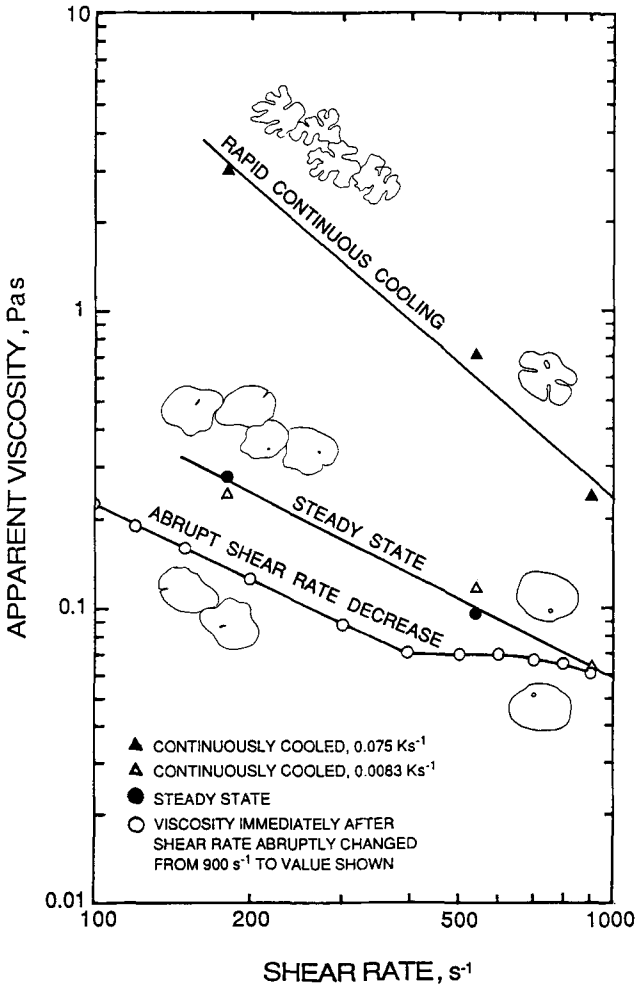

Fig. 25 — Viscosity *vs* shear rate for Al-6.5 wt pct Si alloys at 0.4 fraction solid.[43] Sketches are of microstructures corresponding to the viscosity measurements.

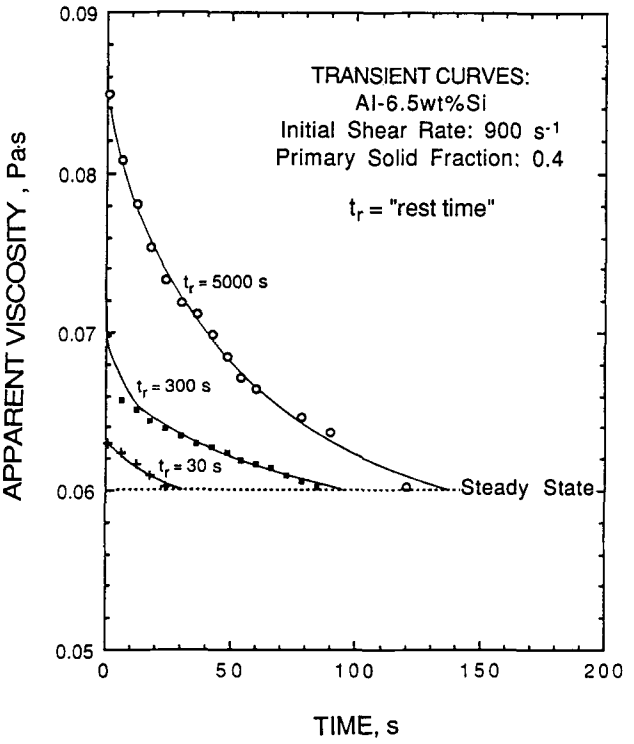

Fig. 26 — Viscosity of Al-6.5 wt pct Si alloy at $\dot{\gamma} = 900\ s^{-1}$ *vs* time after a "rest time," t_r. All samples were at the steady-state viscosity of 0.06 Pa · s at $\dot{\gamma} = 900\ s^{-1}$; shearing was then stopped and restarted at the same shear rate after a time t_r.[43]

is by the area of the hysteresis loop formed when shear stress is increased continuously from zero to some maximum amount and then decreased again to zero. Figure 27 shows examples for Sn-15 pct Pb alloy at 0.4 fraction solid.[41] The alloy was cooled to 0.4 fraction solid under a shear rate of 115 s^{-1} and held isothermally for a total time of 5400 seconds to reach "steady state." Shearing was then stopped, and after a "rest time," t_r, shear rate was increased back to 115 s^{-1} over a time, t_u, and then decreased.

The area under the loop of Figure 27(a) is seen to increase with decreasing t_u from 5 to 2 seconds; for times longer than 5 seconds, the thixotropic effect becomes negligible. Again, only a very short time suffices for "structural breakdown" to reach the steady-state viscosity characteristic of a given shear rate and spheroid size. The picture is, however, quite different for the reverse case, structural buildup. We see in Figure 27(b) that thixotropy continues to increase with increasing "rest time" over the entire range studied (3 to 120 seconds). The structural buildup apparently continues over quite long times.

This structural buildup is further enhanced by solidifying and then partially remelting the semisolid material in the process we have come to call "thixocasting." Measurements on viscosities of "thixocast" Sn-15 pct Pb alloy were made by Laxmanan and Flemings[61] using a modified parallel plate plastometer (essentially a compression test) at low shear rates. Viscosities in the range of 10^7 Pa · s were obtained for material at about 50 pct solid, as shown in Figure 28. These viscosities are many orders of magnitude greater than those obtained for the same alloy with the same initial spheroidal structure after vigorous agitation. Such high viscosities enable small billets to be lifted and handled like solids yet subsequently formed like a viscous liquid (as the viscosity drops during application of shear). A visual example of this behavior is seen in Figure 29. The sample, at about 50 pct solid, retains its strength sufficiently to be handled or "sliced" as shown, yet it is easily deformable under moderate shear.[62]

We have, as yet, little understanding in fundamental detail of how process variables influence viscosity in these semisolid alloys. Such an understanding will be essential to the development of a full constitutive model for the rheological behavior of semisolid slurries. Following Brown,[63] the constitutive relations for these materials might be written

$$\eta = \eta(\dot{\gamma}, f_s, m, s) \quad [4]$$

$$\frac{ds}{dt} = s(\dot{\gamma}, f_s, m, s) \quad [5]$$

where m is a measure of particle morphology and s is a measure of degree of particle agglomeration. Ultimately,

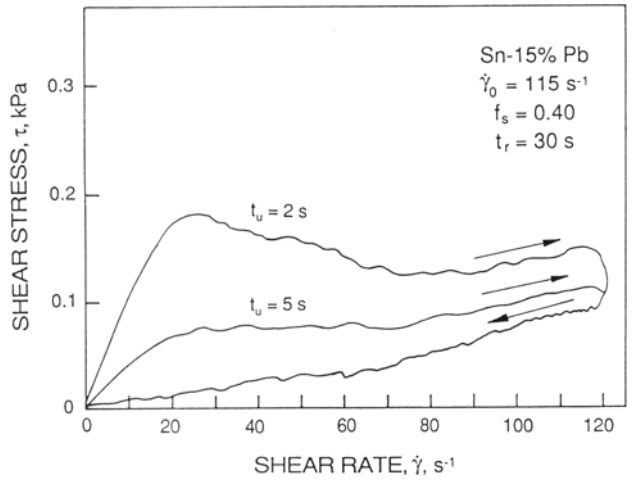

(*a*)

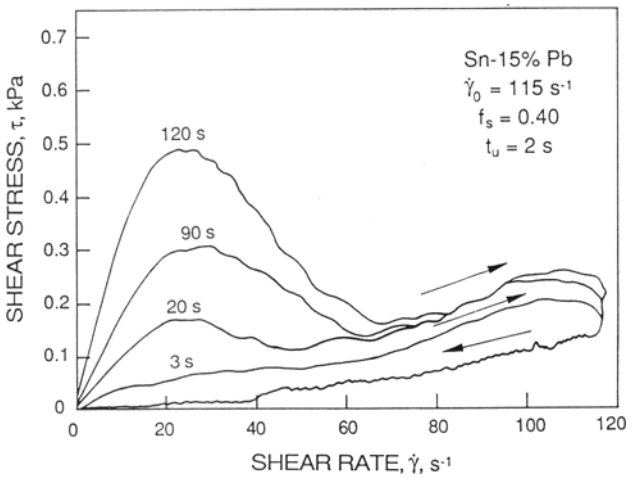

(*b*)

Fig. 27—Thixotropy in Sn-15 wt pct Pb alloy; area enclosed by each curve is a measure of the thixotropy.[42] (*a*) Effect of time to reach maximum shear rate for the "up" portion of the cycle, t_u, and (*b*) effect of rest time, t_r.

we may have to combine constitutive models such as the foregoing with heat and momentum transfer relations relevant to a given process (*e.g.*, with electromagnetic stirring relationships as given by Ilegbusi and Szekely).[64]

C. *Other Metal Alloys*

Results qualitatively similar to those described above for Sn-15 pct Pb alloy and two aluminum alloys have been described for a large number of other aluminum and low melting point alloys, including Al-Cu binary alloys,[47,50,51,52,54,57] Al-Si binary and ternary alloys,[46,48,53] Wood's metal,[49] Al-Pb alloys,[52] Al-Ni alloys,[53] Bi-Sn alloys,[55] Zn-Al alloys,[56] and Al-Zn alloys.[58]

Similar results have also been obtained for a wide range of other metal alloys including copper-base alloys, cast iron, steels, and superalloys. During an extended program at MIT in the 1970's, alloys studied included hypoeutectic cast irons, several copper-base alloys, a cobalt-base superalloy, a nickel-base superalloy, several stainless steels, and a low alloy steel.[65–74]

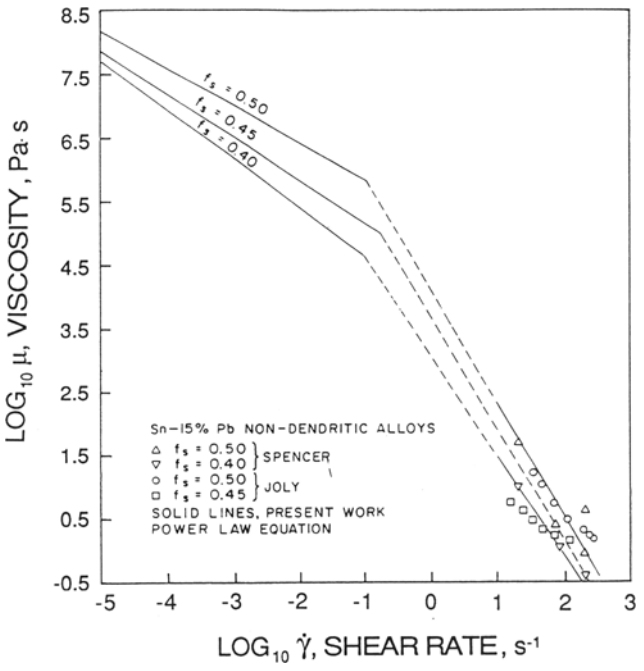

Fig. 28—Viscosity *vs* shear rate for Sn-15 wt pct Pb alloys. Solid lines at the upper left are for "thixocast" materials.[61]

Figure 30 shows viscosity data for a stainless steel and a low alloy steel. Note the similarity of these curves to those given earlier for the tin and aluminum alloys. Structures of several high-temperature "rheocast" alloys are shown in Figure 31. The spheroidal grains shown are also quite similar to those for the lower melting point alloys given earlier.

D. *Composite Materials*

It was recognized early in the rheocasting research at MIT that the high and controllable viscosity of semisolid

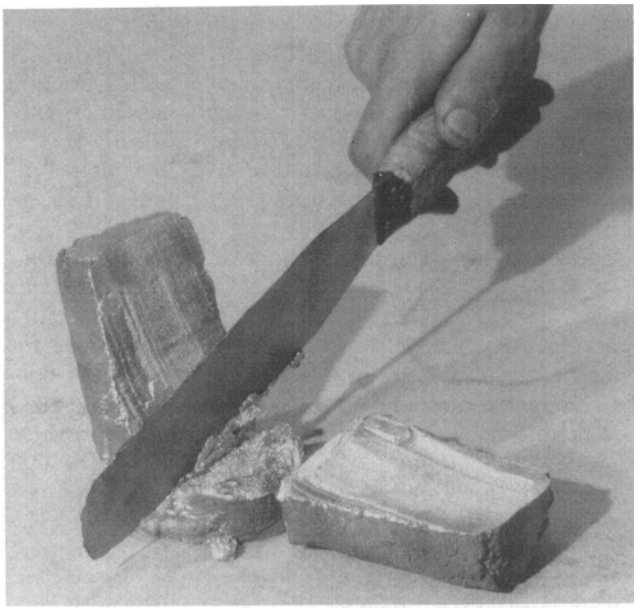

Fig. 29—Semisolid aluminum billet being cut by a spatula[62] (courtesy of ALUMAX Engineered Metal Processes, Inc., St. Louis, MO).

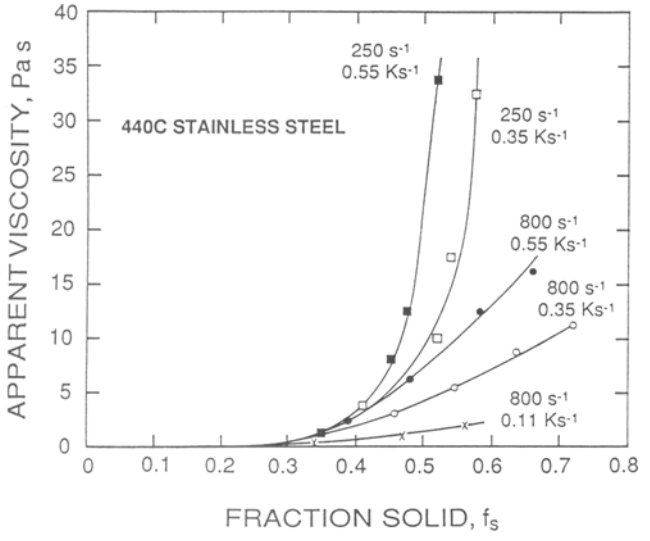

(*a*)

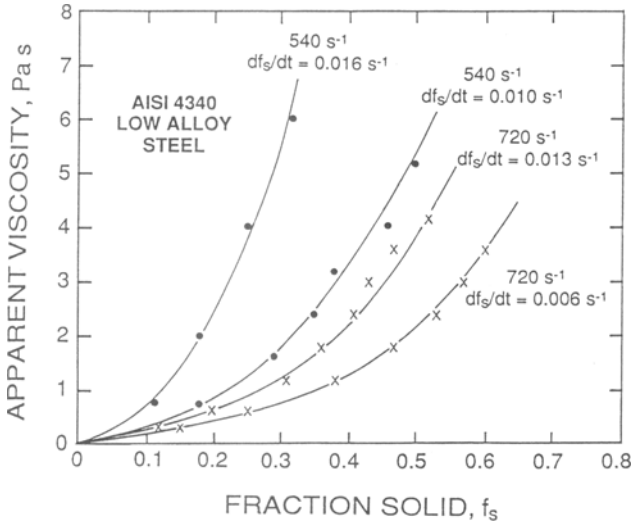

(*b*)

Fig. 30 — Viscosity data for a stainless and a low alloy steel: (*a*) AISI 440C[68] and (*b*) AISI 4340.[69]

slurries made them excellent starting materials for processing metal-matrix composites. It was found that a variety of ceramic particulates could be added to the semisolid slurry and kept in suspension without floating or settling.[75,76] Other researchers have shown that particles can be similarly added to fully liquid metal[77,78] but that a SSM slurry provides better wetting and dispersion.[79] The ease with which particles are entrained in the melt is a sensitive function of surface chemistry (*e.g.*, magnesium in an aluminum alloy greatly aids incorporation and retention of SiC particles, whereas chlorine degassing causes expulsion of the particles).

Rheological properties of these slurry composites have been studied by a number of investigators.[43,80–83] Most find that the composites (with or without partial metal solidification) exhibit thixotropic behavior qualitatively similar to that of partially solidified fully metallic slurries. Figure 32 is an example from recent thesis work of Moon.[43] Figure 32(a) shows viscosity *vs* shear rate for

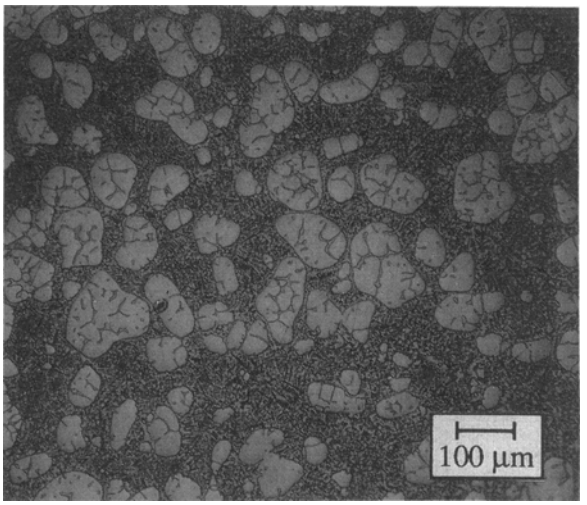

(*a*)

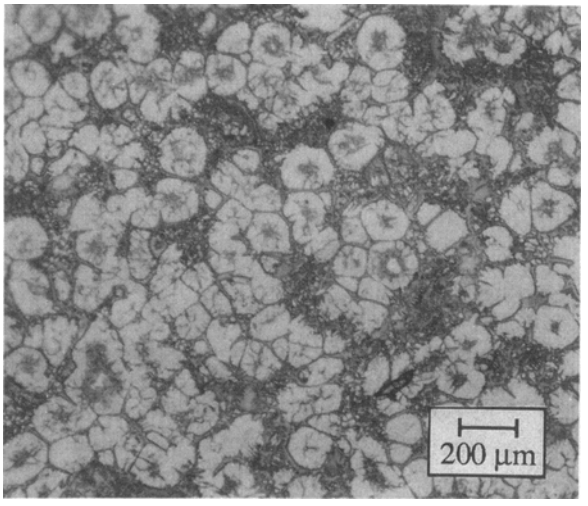

(*b*)

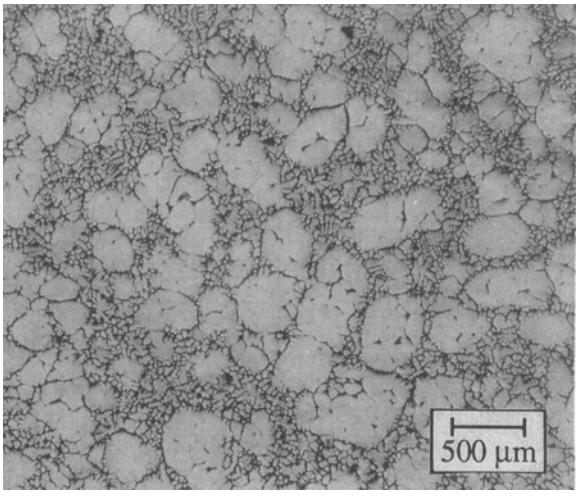

(*c*)

Fig. 31 — Microstructures of some high-temperature alloys: (*a*) a copper alloy, (*b*) stainless steel 440C, and (*c*) low alloy steel AISI 4340.

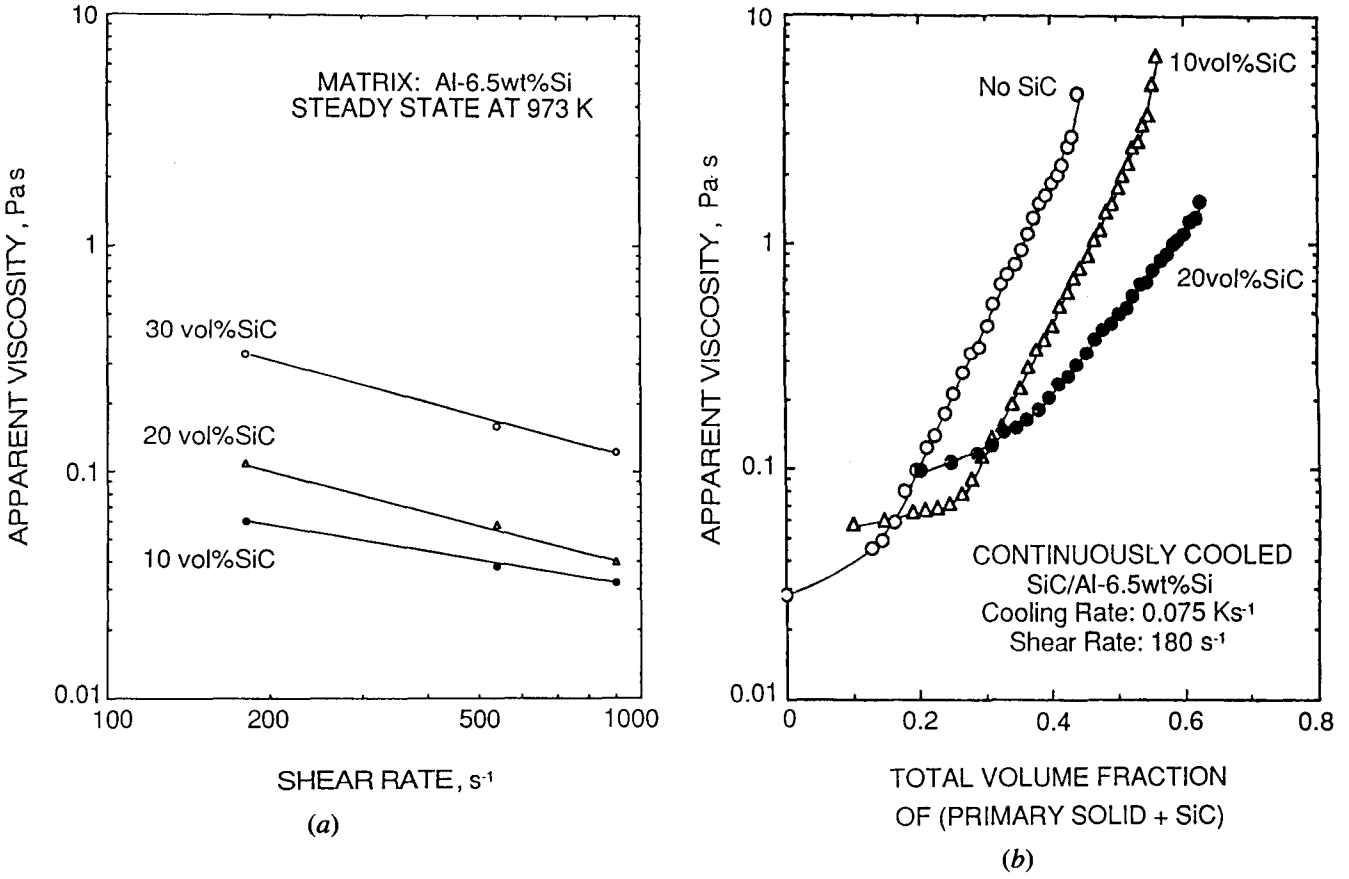

Fig. 32—(*a*) Viscosity of Al-6.5 wt pct Si alloy containing 0, 0.1, and 0.2 volume fraction SiC.[43] (*b*) Viscosity *vs* total volume fraction solid during cooling through the liquid-solid zone of Al-6.5 wt pct Si alloy.

Al-6.5 wt pct Si with 0.1, 0.2, and 0.3 volume fraction SiC. Figure 32(b) shows viscosity during cooling in the liquid-solid range with 0, 0.1, and 0.2 volume fraction SiC. It is of interest that the viscosity for a given total volume fraction of solids is less when a portion of that volume fraction is ceramic particles. This is possibly because the ceramic particles prevent the metal particles from joining and coalescing as readily as in the fully metal slurry. This conclusion is supported by the observation that both the pseudoplasticity and thixotropy appear to be reduced in aluminum slurries by the addition of the particulate SiC. It may also be that the presence of the ceramic accelerates the morphological evolution of the solidified metal particles toward more perfect spheroids. Figure 33 shows typical microstructures of fully metallic and composite slurries from the work of Moon.[43]

E. *Comparison with Familiar Materials and Processes*

We may gain more familiarity with the properties of semisolid metal alloys by comparing them with some well-known materials. Vigorously agitated metals at 40 to 50 pct solid have viscosities typically in the range of 0.1 to 10 Pa · s. This is two to four orders of magnitude higher than the viscosities of water or fully liquid metal and in the range of olive oil, glycerol, and honey (Table I). Yogurt exhibits the same range of viscosities, from about 1 to 10 Pa · s, depending on shear rate. At higher viscosities, molten polymers and molten silicate glass are in the range of 10^3 to 10^4 Pa · s. At these viscosities, materials still flow readily under gravity or moderate pressure.

A material behaves as a "solid" in our vocabulary when it undergoes negligible deformation during a time that is of interest to us. We can begin to handle these semisolid alloys as if they were solids when their viscosity rises much above 10^6 Pa · s, as is seen by the following order of magnitude calculation. A 50-mm cube of semisolid aluminum is imagined to be held between two parallel plates. Gravity produces a shear force. Suppose now that we arbitrarily wish no more displacement than 1 mm in a 10-second period. Required viscosity is estimated simply as the shear force divided by shear rate. The result is a calculated viscosity of approximately 10^6 Pa · s. Semisolid thixocast alloys at 40 to 50 pct or more solid easily reach this viscosity, permitting them to be handled as if they were solids.

The empirical "power law" to describe pseudoplastic behavior of fluids has been given earlier with reference to n, the "power-law index," and K, the "consistency." The smaller the power-law index, the greater the shear thinning effect. Table II lists some typical values of K and n for familiar materials and compares them with some values found for semisolid material. The viscosity of the aluminum alloy used as example (from work of Moon[43])

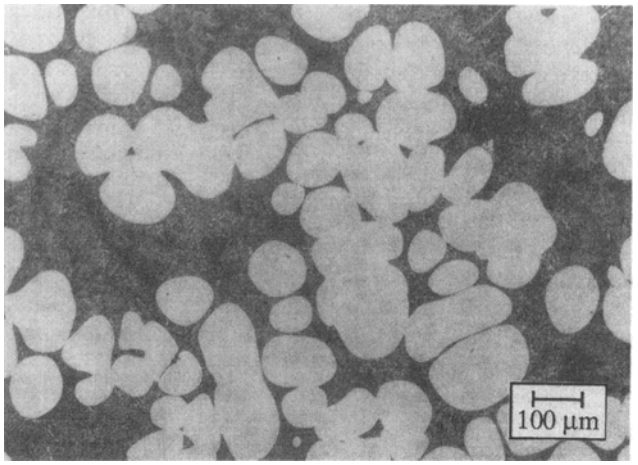

(*a*)

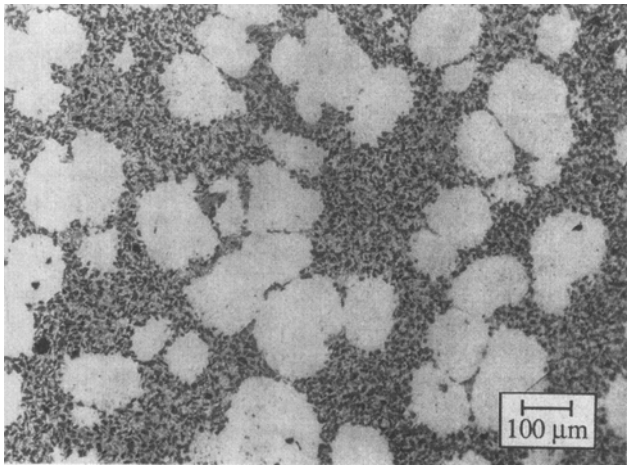

(*b*)

Fig. 33—Semisolid Al-6.5 wt pct Si alloy continuously cooled at 0.075 Ks^{-1} and sheared at 900 s^{-1}:[43] (*a*) matrix alloy only and (*b*) 20 pct SiC added.

has values of K and n at "steady state" that are 30 Pa · (s^n) and 0.1, respectively. These are not far from the values listed for skin cream. For the continuously cooled example, K is much higher (2300 Pa · (s^n)) and n much lower (−0.5), reflecting a more viscous material and, especially, greater shear thinning behavior. This lower n is a result of the irreversible structural changes occurring during cooling, as described earlier. Viscosity of the solidified and partially remelted (thixocast) material of Laxmanan and Flemings[61] at very low shear rate is much higher, with K = 39,800 Pa · (s^n) and n = 0.32.

Data on viscosities of semisolid dendritic alloys which have been obtained are mostly in the range of 10^2 to 10^3 s^{-1}, except for Laxmanan and Flemings'[61] work on thixocast materials which were in the range of shear rate of 10^{-4} to 10^{-2} s^{-1}. Forming processes take place at shear rates over the gamut from superplastic forming at 10^{-3} s^{-1} to explosive forming and die casting at up to 10^4 s^{-1}. Thus, our data to date cover much, but not all, of the range of practical interest (Table III).

Table I. Some Typical Viscosities

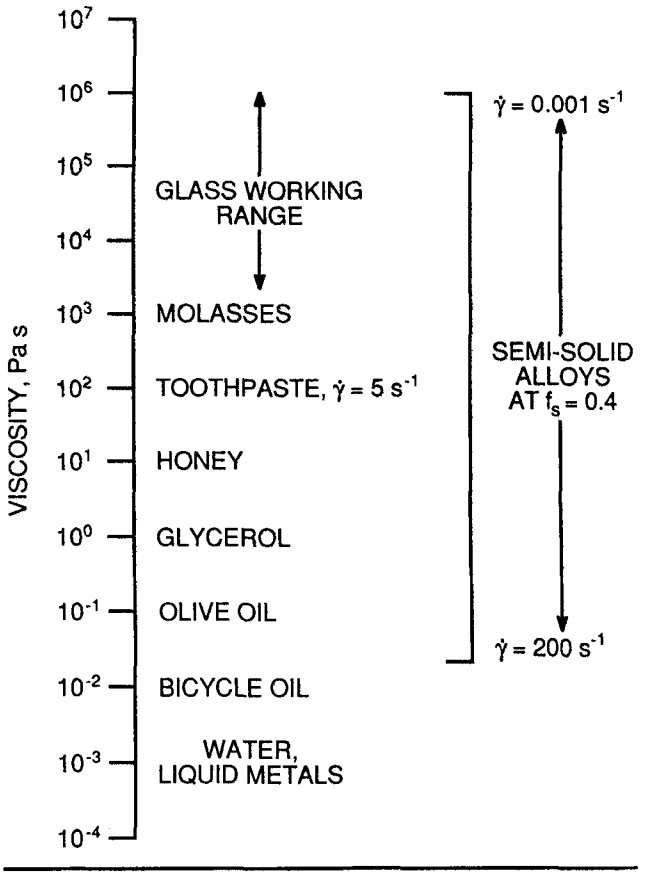

F. *Processes for Achieving Nondendritic Structures*

The main processes used to date for achieving nondendritic structures are illustrated schematically in Figure 34. Figure 34(a) is a simple "batch rheocaster," in which a crucible of molten liquid is mechanically mixed while being cooled. This type of stirrer was used in early MIT work on casting of metal and composite components and in exploratory studies by others. It has been incorporated in vacuum or inert atmosphere chambers for use with high melting point metals or to reduce air entrapment.

A second type of process which has been employed is the "continuous rheocaster" of Figure 34(b), in which (1) higher shear is readily achievable, (2) the stirring is

Table II. Some Materials of Comparable Shear Thinning Behavior

Material	η^*	Viscosity, η, at $\dot{\gamma}$ = 200 s^{-1}
Lubricating grease	0.1	9
Skin cream	0.1	2
Rheocast (Steady state, f_s = 0.4)	0.1	0.3
Yogurt	0.1	0.3

*$\eta = K\dot{\gamma}^{(n-1)}$

Table III. Shear Rates of Familiar Processes

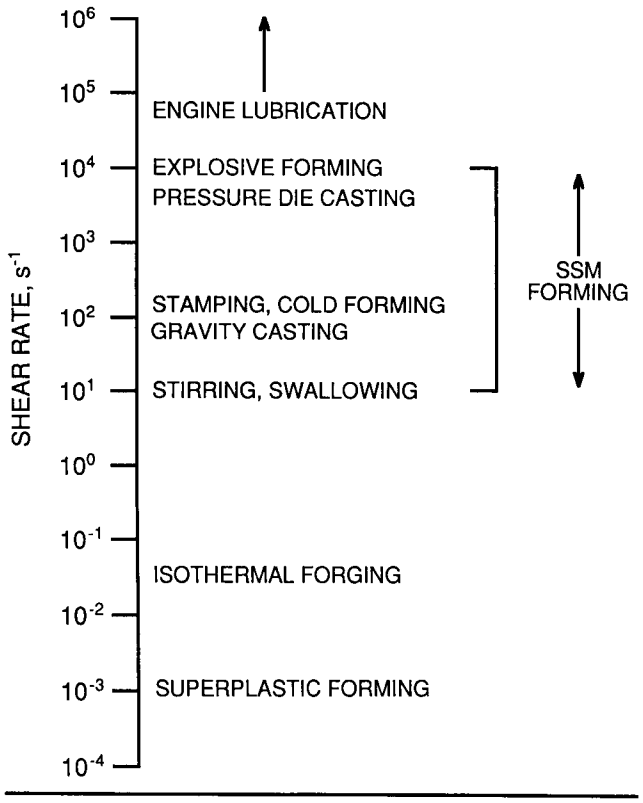

well below the surface of the metal, thus minimizing air entrapment, and (3) cooling rate can be high so as to achieve a fine structure. This type of rheocaster was used in the course of much of the practical process development at MIT for low melting point metals, copper-base alloys, and steels.[65–74,83,84] The third type of process (Figure 34(c)) is vigorous electromagnetic stirring of continuous castings (to produce billets for subsequent thixocasting).[62,85] This is a process of considerable technological importance today, since it permits production of large tonnages using a variant of a well-established technology and it is applicable to high-temperature metals such as steel.

There are other routes as well to production of nondendritic material. In one, the shear is obtained by rapid electromagnetic pulse discharge.[86] In another, the slurry structure is obtained by flow of cooling metal within a tortuous channel to achieve the shear needed for dendritic breakup.[87,88] Another relies solely on long thermal treatment of fine grain structures in the semisolid temperature region; one notable starting material in this process is spray-deposited metal.[89] In still another, the stirring is obtained within the barrel of a machine comparable to an injection molding machine.[90] Nature is kind in a very few alloys, in which the grain refiners employed in usual casting processes are so powerful that the original grain structure is nondendritic. One such case is zirconium-refined magnesium-zinc alloy.[3]

A completely different approach has been termed

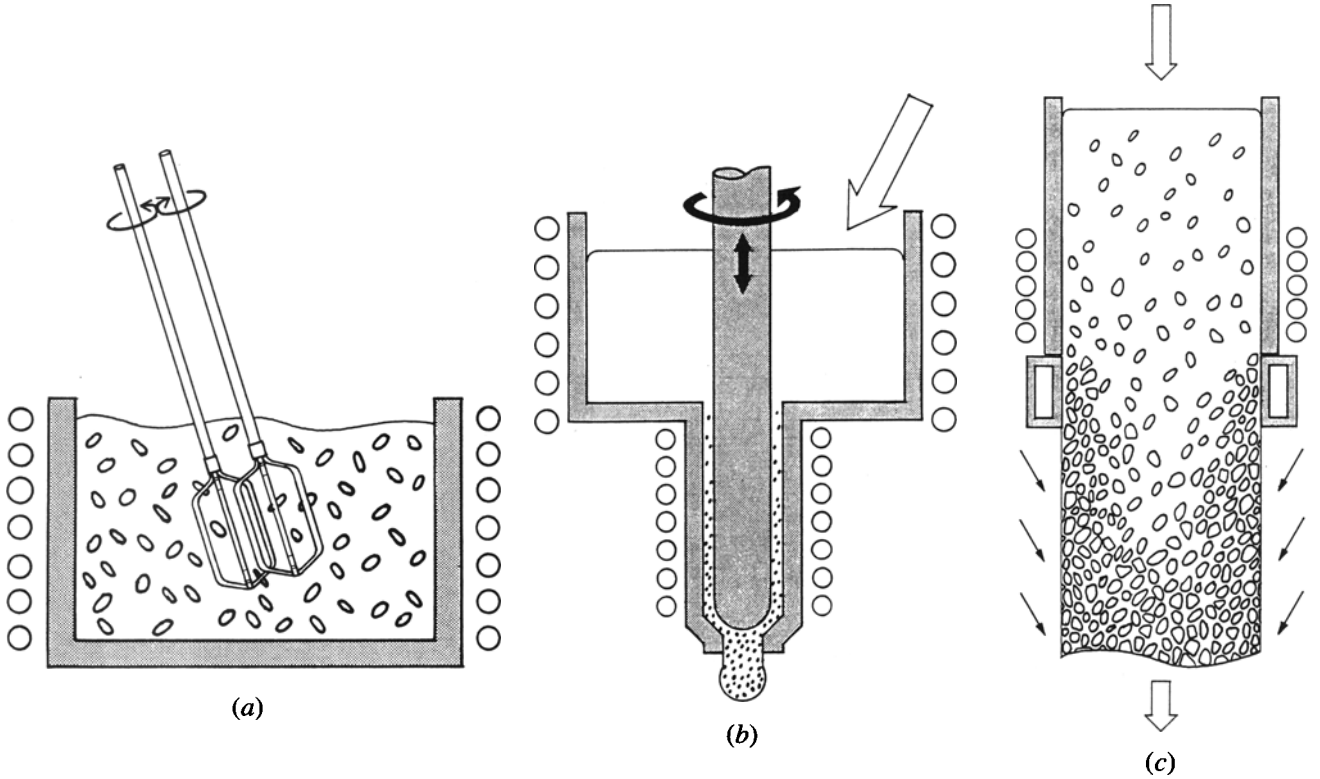

Fig. 34—Schematic diagrams of methods of producing nondendritic structures: (*a*) batch, (*b*) continuous, and (*c*) electromagnetic stirring with continuous casting.

"strain-induced melt activation" (SIMA). In this case, an alloy billet or bar (usually of relatively small cross section) is cold worked a critical amount so that, on reheating into the liquid-solid zone, the desired spheroidal structure is obtained.[62,91] Critical steps in this process appear to be obtaining a fine grain structure in the billet or bar and then achieving grain-boundary melting on reheating. Figure 35 shows the microstructure of an aluminum alloy at three different stages of production of the SIMA material.

At the present time, the only processes in significant commercial usage are electromagnetic stirring of continuous cast ingots ("Magnetohydrodynamic (MHD) process") and the SIMA process. The SIMA process is typically used for diameters under a few centimeters and the MHD process for SSM forming material of larger diameter.

G. *Forming Processes*

The step of solidifying the original slurry in either a continuous casting or shaped casting has been termed "rheocasting." One process under development for direct rheocasting of shapes involves batch stirring a small melt to obtain the correct structure and then centrifuging the slurry into a mold cavity.[92] Another is the "injection molding" process referred to earlier.[90] Processes that seem today to have the most commercial promise are those in which the nondendritic structure is first obtained in continuous cast bar. Small billets cut from the continuous bar are then reheated for subsequent shaping in processes sometimes termed "thixoforming." The process may resemble die casting (Figure 36) or closed die forging (Figure 37), or be a hybrid process in which a forging press is employed, metal enters the mold cavity through a "gate." Other types of processes have also been shown to be suitable for shaping the reheated semisolid material, including extrusion and rolling. A widely used generic term for all these processes today is SSM forming.

Present manufacturing processes, such as those shown schematically in Figures 36 and 37, are now highly automated, with billets being progressively heated under computer control and then transported by robot arms to the forming operation for automatic shaping and subsequent removal from the die. Commercial interest today is primarily in high-integrity aluminum components, especially for the automotive industry. The SSM forming process offers to industry parts of complex shapes that have substantially higher quality than, for example, die castings but are lower in cost than those produced by alternative methods such as forging and machining. The higher quality arises primarily from the higher viscosity of the thixocast material as compared with liquid metal. The SSM can be caused to fill the mold with "solid-front fill," as compared with the metal "spraying" and air entrapment that is endemic to conventional pressure die casting; an example is shown in Figure 38. Improved integrity also results in part from the lower solidification shrinkage of the semisolid alloy.

Plants in operation today for producing SSM parts have no facilities for handling fully molten metal. Their equipment is simply that needed to partially remelt, form, and finish (such as heat-treat) the components. The semisolid material is kept at a low enough fraction liquid that it can be handled as a solid (*e.g.*, with robot arm manipulators). The starting material, the rheocast continuous-cast aluminum alloy, is obtained from one of two smelters now operating in the United States.

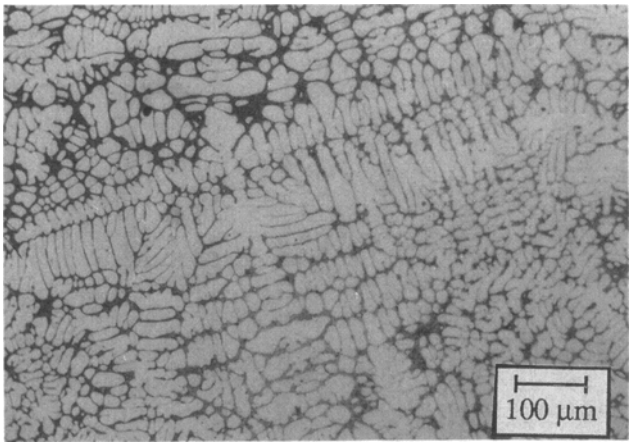

(*a*)

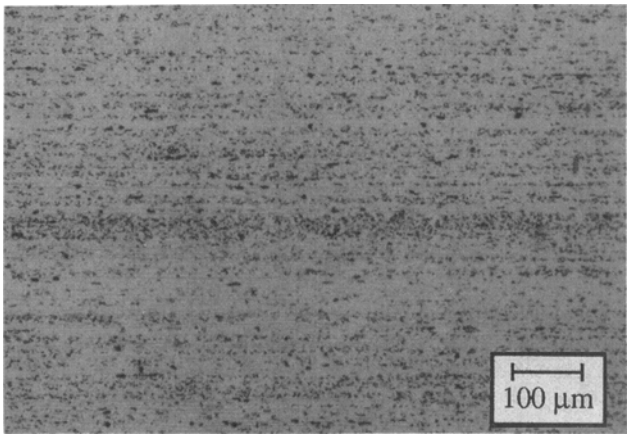

(*b*)

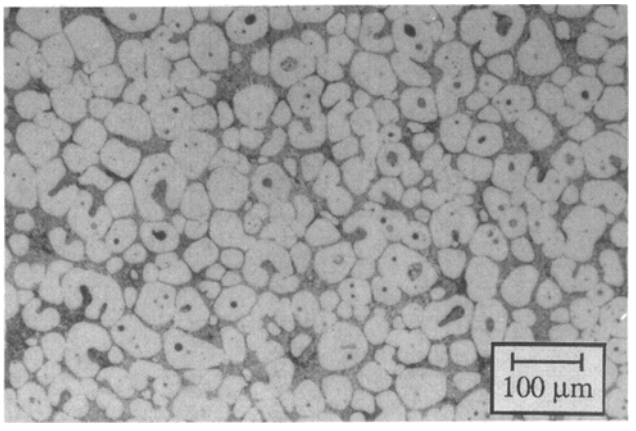

(*c*)

Fig. 35—SIMA processing route for semisolid raw material. Structures shown are of (*a*) original continuous casting, (*b*) extrusion, and (*c*) extrusion after straining and reheating.

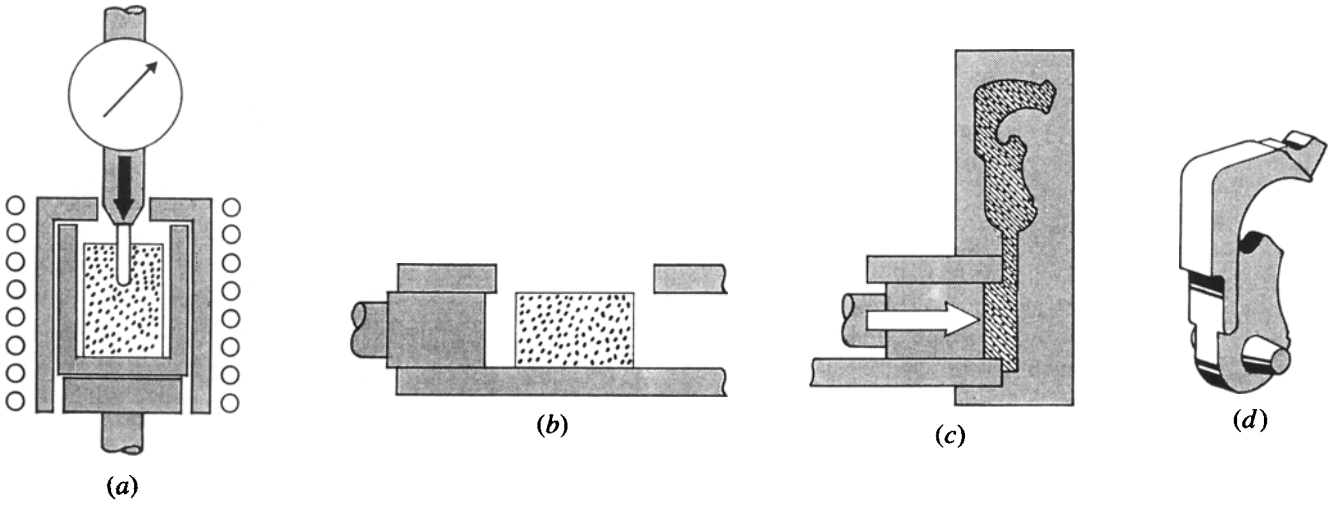

Fig. 36—(*a*) Heating to semisolid state, (*b*) semisolid charge in casting machine, (*c*) die casting, and (*d*) finished part. SSM forming by thixocasting.

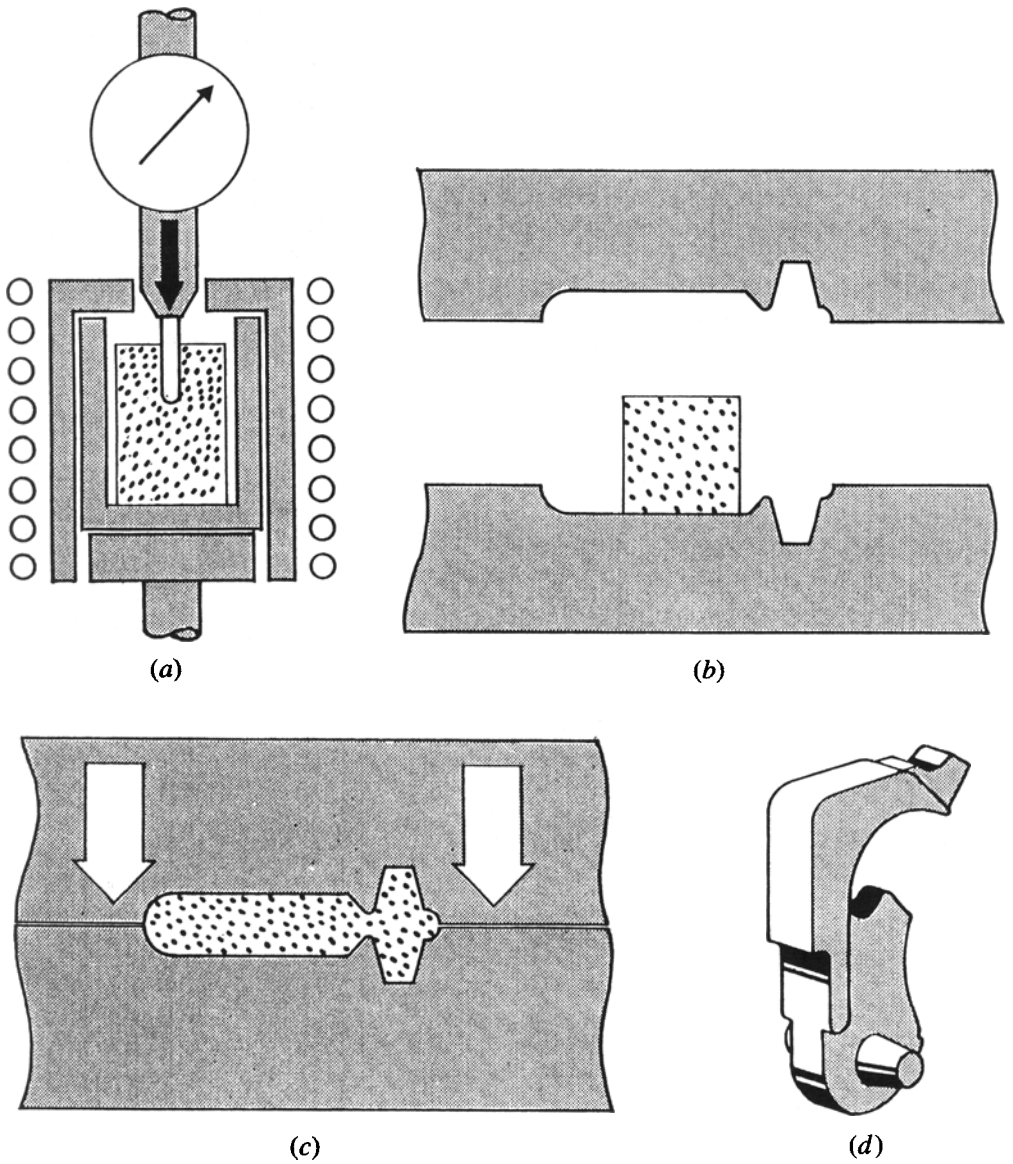

Fig. 37—(*a*) Heating to semisolid state, (*b*) semisolid charge in die, (*c*) forging, and (*d*) finished part. SSM forming by thixoforging.

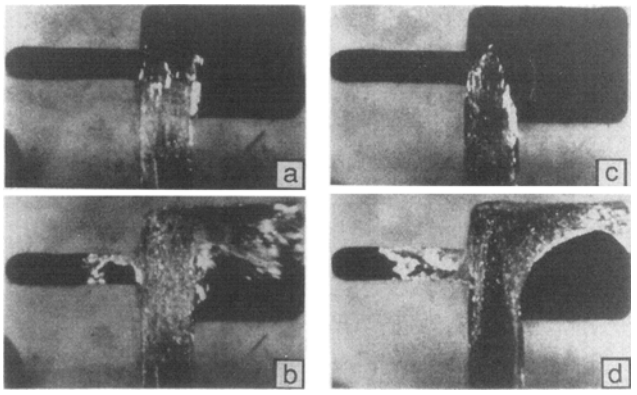

Fig. 38—High-speed photographs of mold filling: (*a*) and (*b*) liquid metal and (*c*) and (*d*) semisolid metal.

One class of parts that has been in production since 1986 is aluminum alloy automotive components. An example is master brake cylinders, such as those shown in Figure 39. These parts are now being produced for a number of European automobiles, and it is anticipated that production will being soon in this country as well. A small pressure-containing component of a brake cylinder is already in production in the United States.

Automotive brake cylinders have traditionally been made of cast iron, but the trend to lighter, more fuel efficient automobiles is favoring a shift to aluminum. Die casting would be the forming method of choice today, except that quality levels obtained are generally found to be unacceptable. Hence, today, most such light alloy cylinders are made from permanent mold castings. Semisolid forming has advantages over permanent molding, in that it can be produced in a highly automated plant with no need to handle liquid metal and it can be made more nearly net shape (Table IV).

Semisolid forging for a typical production cylinder utilizes a two-cavity indirect forming approach and MHD cast alloy 357 slugs cut from 76-mm (3-in.) diameter bar. All major holes are sufficiently cored for tapping or other finishing operations. Mechanical properties of the semisolid forging and the permanent mold casting are comparable. Parts are subjected to a 9.7 MPa (1400 psi) nitrogen leak test and extensive endurance testing, which includes 300,000 to 1 million hydraulic cycles that must be endured without a sign of wear.[62]

Another class of automotive parts for which production is anticipated is that of steering and suspension system components. Examples are shown in Figure 40. Other

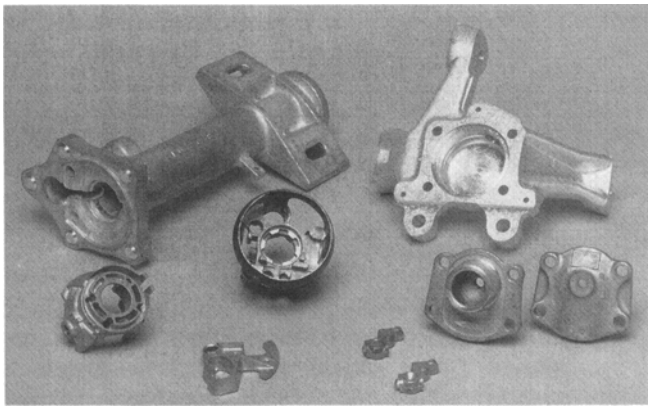

Fig. 40—Aluminum alloy automotive steering and suspension system components produced by SSM forming (courtesy of ALUMAX Engineered Metal Processes, Inc., St. Louis, MO).

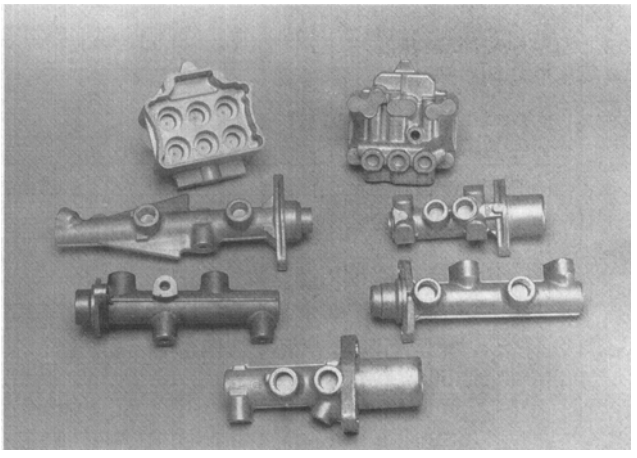

Fig. 39—Aluminum alloy automotive brake system components produced by semisolid forging (courtesy of ALUMAX Engineered Metal Processes, Inc., St. Louis, MO).

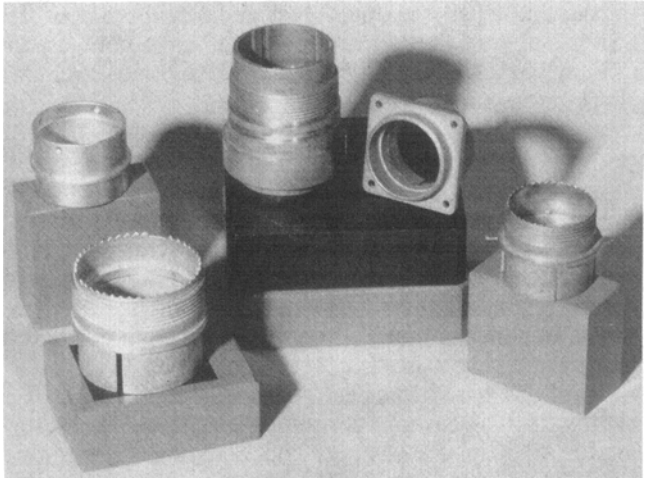

Fig. 41—Aluminum alloy 6262 electrical connectors produced by semisolid forging (courtesy of ALUMAX Engineered Metal Processes, Inc., St. Louis, MO).

Table IV. Part Mass and Production Rate for a Master Brake Cylinder

Process	Aluminum Alloy	Mass as Formed, g	Finished Part Mass, g	Machining Loss, Pct	Production Rate Pieces per Mold per Hour
SSM	357-T5	450	390	13	150
Permanent mold cast	356-T6	760	450	40	24

Table V. Part Mass and Production Rate of an Electrical Connector

Process	Aluminum Alloy	Raw Material Mass, g	Finished Part Mass, g	Machining Loss, Pct	Production Rate (Primary Operation) Pieces per Hour
SSM	6262-T6	25	23	8	300
Machining	6262-T9	245	23	81	200

potential areas of application are rocker arms, engine pistons, wheels, transmission components, fuel systems, and air conditioner components.

Another class of parts, one which has been in production since 1981, is that of electrical connectors for military aerospace applications (Figure 41).[62,93] Qualification of these parts involves extensive functional testing under various environmental conditions. Production quality control procedures are stringent to ensure conformance to specifications and performance under load.

Before semisolid forging, these parts were machined (on screw machines) from extruded aluminum alloy 6262-T9 bar. Today, a large number of these parts are semisolid forged from SIMA 6262 bar and finish machined after a T6 heat treatment. The characteristics of semisolid forged and machined parts are compared in Table V. The semisolid forged component possesses all major keyways and locating devices with tolerances at least equivalent to machined parts. The savings in material, plus the higher production rate, make the semisolid forged part an economical selection.

After full T6 heat treatment, the parts are finish machined and anodized. They are tested per MIL-C-38999 and meet all specified performance criteria. These tests include bending, vibration, durability, thermal shock, and impact and tensile testing. Mechanical properties of the SSM and of the forged material are comparable (350 MPa tensile strength, 280 MPa yield strength, 10 pct elongation).

H. *Properties and Characteristics for Future Exploitation*

One can envision the extension of the semisolid forming process well beyond the limits within which it is commercially employed today. A convenient way to do this is to consider some of the properties and characteristics of SSM, as listed in Table VI.

The SSM has lower heat content, thus requiring less energy than die casting, permitting higher speed part formation than in die casting, and potentially permitting practical development of a "ferrous die casting process."

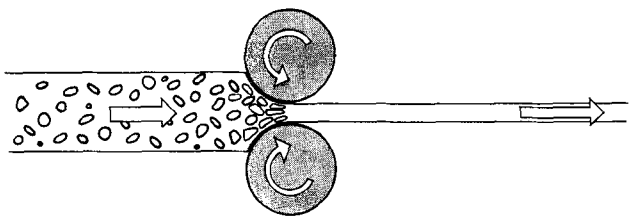

Fig. 42—Schematic diagram of a possible strip casting process using SSM technology.

The fact that viscosity can be controlled over a range of many orders of magnitude opens doors to improved processes and products and to wholly new processes. In comparison with liquid metal casting processes, the presence of some solid in the metal to be formed presents unique advantages. And, of course, in comparison with solid metal forming, the lower flow stress of semisolid forming opens up new processing vistas.

One potential area of application of SSM technology being considered in several locations is casting of strip, especially steel strip. A commercially viable process for direct casting of carbon steel strip is being sought in major research laboratories throughout the world. The lower

Table VI. Properties and Characteristics for Further Exploitation

Characteristic	Potential Benefit or Application
SSM has lower heat content than liquid metal	higher speed part forming higher speed continuous casting lower mold erosion lower energy consumption ferrous part forming forming of other high melting point materials
Viscosity higher in SSM than in liquid metals; viscosity can be varied as required	improved mold filling: "solid front" reduced oxides—improved machinability less gas entrapment improved soundness less mold attack higher speed part forming improved surface finish automation new processes
Solid is present in SSM at time of mold filling	less casting shrinkage, fewer voids less "feeding" required less macrosegregation fine grain structure
Flow stress lower in SSM than in solid metal	forming of intricate parts higher speed part forming lower cost part forming high-speed forming of continuous shapes (*e.g.*, extrusion) new processes
Ability to incorporate other materials	composites
Ability to separate liquid from solid	purification

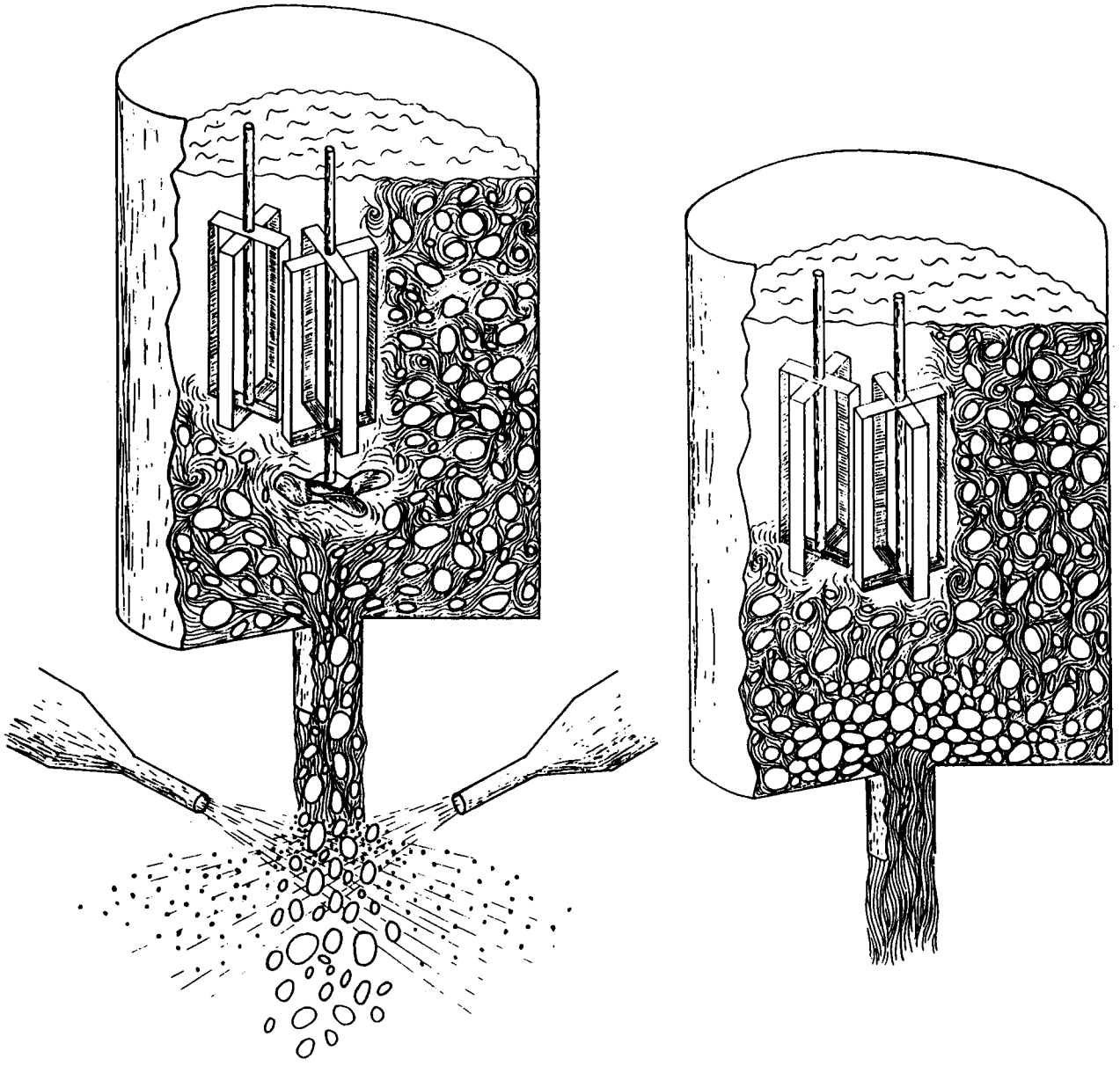

(a) (b)

Fig. 43—(*a*) and (*b*) Refining by SSM technology.[92]

heat content, unique structure, and rheological properties of semisolid nondendritic material may provide a potential route to such a process. Figure 42, based on thesis research of Matsumiya and Flemings,[94] illustrates one way such a process might look.

There is much current interest as well today in applying SSM technology to forming of composite materials, as discussed earlier. Finally, as illustrated schematically in Figure 43, the basic technology provides a potential means of metal purification,[95] by either (1) atomization of a semisolid slurry with subsequent segregation by particle size or (2) draining liquid from a slurry through an appropriate coarse filter.[95]

The original discovery of rheocasting was made nearly 20 years ago in the doctoral thesis of Speencer.[40] We have come a long way in the intervening years in our understanding of the fundamentals of the process and of its practical application. It seems likely that the progress will be much greater in the next 20 years, from the standpoints of both fundamental understanding and industrial practice.

ACKNOWLEDGMENTS

Funding for the early work on isothermal rheological behavior of SSM's, that led to and included the basic discovery by Spencer in 1971, was from the American Foundrymen's Society, the Army Research Office, and the Office of Naval Research. Scaleup and application to steel were sponsored by the Defense Advanced Research Projects Agency (DARPA). Following the hot tearing work of Metz and Flemings,[24,25] and Spencer's subsequent discovery,[40] contributions to the

fundamental understanding and to the development of the rheocasting process were made by a large number of investigators at MIT and elsewhere, as described in this paper. Major contributors at MIT included P. Joly, V. Laxmanan, T. Matsumiya, R. Mehrabian, H.-K. Moon, R. Riek, and K.P. Young. Many others contributed as well, and the work of some of them may prove to be of much future importance. Those individuals who have been co-authors of papers on the process, and not mentioned above are, in alphabetical order, D.G. Backman, B.E. Bond, J.F. Boylan, P.O. Charreyron, J.A. Cornie, E.F. Fascetta, D.R. Geiger, T.Z. Kattamis, N. Matsumoto, M. Nakada, T.J. Piccone, D.A. Pinsky, A. Sato, A. Shibutani, and Y. Shiohara. The majority of these individuals were graduate students at the time of their contributions. Special acknowledgment is due to Dr. T.J. Piccone, who has both contributed to the rheocasting technology and has helped greatly in preparation of this manuscript. Finally, thanks are due to Mr. M.P. Kenney of ALUMAX Engineered Metal Processes, Inc., St. Louis, MO, and to Dr. K.P. Young of AMAX Research and Development Center, Golden, CO, for supplying data and figures relating to current industrial practice.

REFERENCES

1. T.F. Bower, H.D. Brody, and M.C. Flemings: *Trans. AIME*, 1966, vol. 236, pp. 624-34.
2. H.D. Brody and M.C. Flemings: *Trans. AIME*, 1966, vol. 236, pp. 615-24.
3. M.C. Flemings: *Solidification Processing*, McGraw-Hill Book Company, New York, NY, 1974.
4. I. Ohnaka: *Trans. Iron Steel Inst. Jpn.*, 1986, vol. 26, pp. 1045-51.
5. T.W. Clyne and W. Kurz: *Metall. Trans. A*, 1981, vol. 12A, pp. 965-71.
6. S. Kobayashi: *J. Cryst. Growth*, 1988, vol. 88, pp. 87-96.
7. D.H. Kirkwood: *Mater. Sci. Eng.*, 1984, vol. 65, pp. 101-09.
8. A.J.W. Ogilvy and D.H. Kirkwood: *Appl. Sci. Res.*, 1987, vol. 44, pp. 43-49.
9. A. Mortensen: *Metall. Trans. A*, 1989, vol. 20A, pp. 247-53.
10. T.W. Clyne: *Met. Sci.*, 1982, vol. 16, pp. 441-50.
11. M.C.M. Cornelissen: *Ironmaking and Steelmaking*, 1986, vol. 13, pp. 204-12.
12. K.S. Yeum, V. Laxmanan, and D.R. Poirier: *Metall. Trans. A*, 1989, vol. 20A, pp. 2847-56.
13. J.K. Chuang, D. Reinisch, and K. Schwerdtfeger: *Metall. Trans. A*, 1975, vol. 6A, pp. 235-38.
14. Y. Ueshima, S. Mizoguchi, T. Matsumiya, and H. Kajioka: *Metall. Trans. B*, 1986, vol. 17B, pp. 845-59.
15. S. Mizoguchi, Y. Ueshima, T. Matsumiya, and H. Kajioka: *Solidification Processing 1987*, Institute of Metals, London, pp. 75-78.
16. A.M. Michael and M.B. Bever: *Trans. AIME*, 1954, vol. 200, pp. 47-56.
17. W. Kurz, B. Giovanola, and R. Trivedi: *Acta Metall.*, 1986, vol. 34, pp. 823-30.
18. B. Giovanola and W. Kurz: *Metall. Trans. A*, 1990, vol. 21A, pp. 260-63.
19. A.J. Campagna: Ph.D. Thesis, Massachusetts Institute of Technology, Cambridge, MA, 1970.
20. M.C. Flemings: *F. Weinberg Int. Conf. on Solidification Processing*, J.E. Lait and I.V. Samarasekera, eds., Pergamon Press, New York, NY, 1990, pp. 173-94.
21. T.Z. Kattamis, J.C. Coughlin, and M.C. Flemings: *Trans. AIME*, 1967, vol. 239, pp. 1504-11.
22. H. Jones: *J. Mater. Sci.*, 1984, vol. 19, pp. 1043-76.
23. T.Z. Kattamis and M.C. Flemings: *Trans. AIME*, 1965, vol. 233, pp. 992-99.
24. S.A. Metz and M.C. Flemings: *Trans. Am. Foundrymen's Soc.*, 1969, vol. 77, pp. 329-34.
25. S.A. Metz and M.C. Flemings: *Trans. Am. Foundrymen's Soc.*, 1970, vol. 78, pp. 453-60.
26. D.B. Spencer, R. Mehrabian, and M.C. Flemings: *Metall. Trans.*, 1972, vol. 3, pp. 1925-32.
27. R.A. Rosenberg, M.C. Flemings, and H.F. Taylor: *Trans. Am. Foundrymen's Soc.*, 1960, vol. 28, pp. 518-28.
28. T.W. Clyne and G.J. Davies: *Solidification and Casting of Metals*, The Metals Society, London, 1979, pp. 275-78.
29. K. Miyazawa and K. Schwerdtfeger: *Arch. Eisenhuettenwes.*, 1981, vol. 52, pp. 415-22.
30. M.C. Flemings and G.E. Nereo: *Trans. AIME*, 1967, vol. 239, pp. 1449-61.
31. R.S. Richards and W. Rostoker: *Trans. ASM*, 1956, vol. 48, pp. 884-903.
32. R.T. Southin: *J. Inst. Met.*, 1966, vol. 94, pp. 401-07.
33. G. Schmid and A. Roll: *Z. Elektrochem.*, 1939, vol. 45, pp. 769-75.
34. D.R. Uhlmann, T.P. Seward III, and B. Chalmers: *Trans. AIME*, 1966, vol. 236, pp. 527-31.
35. T.F. Bower and M.C. Flemings: *Trans. AIME*, 1967, vol. 239, pp. 216-19.
36. H. Garabedian and R.F. Strickland-Constable: *J. Cryst. Growth*, 1974, vol. 22, pp. 188-92.
37. H. Garabedian and R.F. Strickland-Constable: *J. Cryst. Growth*, 1972, vol. 13/14, pp. 506-09.
38. A. Vogel: *Met. Sci.*, 1978, vol. 12, pp. 576-78.
39. N. Apaydin, K.V. Prabhakar, and R.D. Doherty: *Mater. Sci. Eng.*, 1980, vol. 46, pp. 145-50.
40. D.B. Spencer: Ph.D. Thesis, Massachusetts Institute of Technology, Cambridge, MA, 1971.
41. P.A. Joly: Ph.D. Thesis, Massachusetts Institute of Technology, Cambridge, MA, 1974.
42. P.A. Joly and R. Mehrabian: *J. Mater. Sci.*, 1976, vol. 11, pp. 1393-1418.
43. H.-K. Moon: Ph.D. Thesis, Massachusetts Institute of Technology, Cambridge, MA, 1990.
44. M.C. Flemings: *Rheocasting*, Proc. of the Workshop on Rheocasting, Army Materials and Mechanics Research Center, Watertown, MA, Feb. 3–4, 1977, R.D. French and Frank S. Hodi, eds, Metals and Ceramics Information Center, Columbus, OH, pp. 33-39.
45. T.Z. Kattamis and T.J. Piccone: *Mater. Sci. Eng.*, 1991, vol. A131, pp. 265-72.
46. W.R. Loue and W.H. Kool: Laboratory of Materials Science and Technology, Delft University of Technology, Delft, The Netherlands, 1989, private communications.
47. A. Shibutani, K. Arihara, and Y. Nakamura: *Tetsu-to-Hagané*, 1980, vol. 66, pp. 1550-56.
48. K. Miwa and R. Ichikawa: *J. Jpn. Inst. Met.*, 1981, vol. 45, pp. 853-59.
49. K. Chizawa and S. Fukuoka: *J. Fac. Eng. Univ. Tokyo*, 1975, vol. 33 (2), pp. 149-66.
50. R. Ichikawa and K. Miwa: *J. Jpn. Inst. Met.*, 1981, vol. 45, pp. 189-93.
51. N. Mori, K. Ogi, and K. Matsuda: *J. Jpn. Inst. Met.*, 1984, vol. 48, pp. 936-44.
52. K. Ichikawa and S. Ishizuka: *Trans. Jpn. Inst. Met.*, 1987, vol. 28 (2), pp. 145-53.
53. K. Ichikawa, S. Ishizuka, and Y. Kinoshita: *Trans. Jpn. Inst. Met.*, 1988, vol. 29 (7), pp. 598-607.
54. K. Ichikawa, S. Ishizuka, and Y. Kinoshita: *Trans. Jpn. Inst. Met.*, 1987, vol. 28 (2), pp. 135-44.
55. M.A. Taha, N.A. Mahallawy, M. Lofty Zamzam, and S. El-Mardy: *Solidification Processing 1987*, Institute of Metals, London, pp. 409-12.
56. H. Lehuy, J. Masounave, and J. Blain: *J. Mater. Sci.*, 1985, vol. 20, pp. 105-13.
57. H.I. Lee: Ph.D. Thesis, University of Sussex, Sussex, United Kingdom, 1982.
58. N. Wang, G. Shu, and H. Yang: *Proc. Int. Symp. on New Developments in Cast Alloy Technology*, B. Liu and J. Liu, eds., Luoyang, People's Republic of China, 1988.
59. W.R. Loue, E. Nava-Vazquez, and W.H. Kool: *1st Int. Conf. on Semi-Solid Processing of Alloys and Composites*, April 4–6,

1990, Ecole Nationale Superior des Mines de Paris, Sophia-Antipolis, Valbonne, France.
60. H.A. Rames, J.F. Hutton, and K. Walters: *An Introduction to Rheology*, Elsevier Science Publishers, New York, NY, 1989.
61. V. Laxmanan and M.C. Flemings: *Metall. Trans. A*, 1980, vol. 11A, pp. 1927-37.
62. M.P. Kenney, J.A. Courtois, R.D. Evans, G.M. Farrier, C.P. Kyonka, A.A. Koch, and K.P. Young: *Metals Handbook, 9th ed.*, ASM INTERNATIONAL, Metals Park, OH, 1988, vol. 15, pp. 327-38.
63. S.B. Brown: *Proc. 5th Int. Conf. on the Modeling of Casting, Welding, and Solidification Processes*, M. Rappaz, ed., TMS, Warrendale, PA, 1990.
64. O.J. Ilegbusi and J. Szekely: *Iron Steel Inst. Jpn. International*, 1990, vol. 30 (5), pp. 372-80.
65. M.C. Flemings *et al.*: *Machine Casting of Ferrous Alloys*, Interim Technical Report, ARPA Contract No. DAAG46-73-C-0110, Dec. 1973.
66. M.C. Flemings *et al.*: *Machine Casting of Ferrous Alloys*, Interim Technical Report, ARPA Contract No. DAAG46-73-C-0110, Dec. 1974.
67. M.C. Flemings, R. Mehrabian, J.R. Melcher, R.G. Riek, K.P. Young, N. Matsumoto, D.G. Backman, F.S. Blackall, B.E. Bond, E. McHale, and F.S. Schottman: *Machine Casting of Ferrous Alloys*, Interim Technical Report, ARPA Contract No. DAAG46-73-C-0110, June 1975.
68. M.C. Flemings, K.P. Young, and R.G. Riek: *Machine Casting of Ferrous Alloys*, Interim Technical Report, ARPA Contract No. DAAG46-73-C-0110, Dec. 1975.
69. M.C. Flemings, K.P. Young, R.G. Riek, J.F. Boylan, and R.L. Bye: *Machine Casting of Ferrous Alloys*, Interim Technical Report, ARPA Contract No. DAAG46-73-C-0110, June 1976.
70. M.C. Flemings, K.P. Young, J.F. Boylan, R.L. Bye, M.L. Santor, and B.E. Bond: *Machine Casting of Ferrous Alloys*, Interim Technical Report, ARPA Contract No. DAAG46-73-C-0110, June 1977.
71. M.C. Flemings, J.F. Boylan, and R.L. Bye: *Thixocasting Steel Parts*, Final Technical Report, ARPA Contract No. DAAG46-77-C-0033, Sept. 1978.
72. M.C. Flemings and R. Mehrabian: *Trans. Int. Foundry Congress*, Moscow, 1973, *Trans. Am. Foundrymen's Soc.*, 1973, vol. 81, pp. 81-88.
73. M.C. Flemings, R.G. Riek, and K.P. Young: *Mater. Sci. Eng.*, 1976, vol. 25, pp. 103-17.
74. M.C. Flemings and K.P. Young: *Yearbook of Science and Technology*, McGraw Hill Book Company, New York, NY, 1978, pp. 49-58.
75. R. Mehrabian, R.G. Riek, and M.C. Flemings: *Metall. Trans. A*, 1974, vol. 5A, pp. 1899-1905.
76. M.C. Flemings, R.G. Riek, and K.P. Young: *Am. Foundrymen's Soc. Int. Cast. Met. J.*, 1976, vol. 3, pp. 11-22.
77. P.K. Rohatgi, B.C. Pai, and S.C. Panda: *J. Mater. Sci.*, 1979, vol. 14, pp. 2277-83.
78. P.K. Rohatgi, R. Asthana, and S. Das: *Int. Met. Rev.*, 1986, vol. 31, pp. 115-39.
79. J.W. McCoy, C. Jones, and F.E. Wawner: *SAMPE Q.*, 1988, vol. 19 (2), pp. 37-50.
80. G. Girot: Doctoral Thesis, L'Université de Bordeaux I, Bordeaux, France, 1987.
81. W.R. Loue and W.H. Kool: Laboratory of Materials Science and Technology, Delft University of Technology, Delft, The Netherlands, private communications, 1989.
82. M. Mada and F. Ajersch: Abstract, TMS Annual Meeting, Anaheim, CA, Feb. 1990.
83. R.G. Riek, K.P. Young, N. Matsumoto, R. Mehrabian, and M.C. Flemings: *Society of Die Casting Engineers 1975 Trans.*, 8th Int. Die Casting Exposition and Congress, Detroit, MI, Paper No. G-T75-153.
84. K.P. Young, R.G. Riek, J.F. Boylan, R.L. Bye, B.E. Bond, and M.C. Flemings: *Trans. Am. Foundrymen's Soc.*, 1976, vol. 84, pp. 169-74; *Die Casting Engineer*, Mar.–Apr. 1976, pp. 46-52.
85. K.P. Young, D.E. Tyler, H.P. Cheskis, and W.G. Watson: U.S. Patent 4,482,012, 1984.
86. M. Nakada, Y. Shiohara, and M.C. Flemings: *Iron Steel Inst. Jpn. Int.*, 1990, vol. 30, pp. 27-33.
87. G.B. Brook: *Mater. Design*, 1982, vol. 3, pp. 558-65.
88. R.L. Antona and R. Moschini: *Met. Sci. Technol.*, 1986, vol. 4 (2), pp. 49-59.
89. A.J.W. Ogilvy: Osprey Metals Ltd., Glamorgan, United Kingdom, private communication, 1990.
90. P.S. Frederick, N.L. Bradley, and S.C. Erickson: *Advanced Materials and Processes*, 1988, vol. 134 (4), pp. 53-56.
91. K.P. Young, C.P. Kyonka, and J.A. Courtois: U.S. Patent 4,415,374, 1983.
92. J. Collot, U.S. Patent No. 4510987, April 16, 1985.
93. P.S. Wilcox: Abstract, *1st Int. Conf. on Semi-Solid Processing of Alloys and Composites*, Sophia-Antipolis, France, Apr. 4–6, 1990.
94. T. Matsumiya and M.C. Flemings: *Metall. Trans. B*, 1981, vol. 12B, pp. 17-31.
95. R. Mehrabian, D.R. Geiger, and M.C. Flemings: *Metall. Trans.*, 1974, vol. 5, pp. 785-87.